Aram Dorsum: an extensive mid-Noachian age fluvial depositional system in Arabia Terra, Mars

JGR Planets

RESEARCH ARTICLE
10.1029/2019JE006244

Key Points:
- Aram Dorsum (AD) is an ~85 km long, branching, flat-topped ridge with layered flanks in Arabia Terra, Mars
- AD is an exhumed aggradational river system with floodplains deposits and was probably active for 10^5–10^7 years in the mid-Noachian
- The AD rivers were sourced both locally and regionally, indicating that the ancient Martian climate supported precipitation and runoff here

Supporting Information:
- Supporting Information S1

Correspondence to:
M. R. Balme,
matt.balme@open.ac.uk

Citation:
Balme, M. R., Gupta, S., Davis, J. M., Fawdon, P., Grindrod, P. M., Bridges, J. C., et al. (2020). Aram Dorsum: An extensive mid-Noachian age fluvial depositional system in Arabia Terra, Mars. *Journal of Geophysical Research: Planets*, *125*, e2019JE006244. https://doi.org/10.1029/2019JE006244

Received 21 OCT 2019
Accepted 25 MAR 2020
Accepted article online 15 APR 2020

Author Contributions:
Conceptualization: Matthew R. Balme
Formal analysis: Matthew R. Balme
Funding acquisition: Matthew R. Balme, Peter M. Grindrod, John C. Bridges
Investigation: Matthew R. Balme, Sanjeev Gupta, Joel M. Davis, Peter Fawdon, Peter M. Grindrod, John C. Bridges, Rebecca M. E. Williams
Methodology: Matthew R. Balme, Peter Fawdon
Project administration: Matthew R. Balme
(continued)

Aram Dorsum: An Extensive Mid-Noachian Age Fluvial Depositional System in Arabia Terra, Mars

Matthew R. Balme[1], Sanjeev Gupta[2], Joel M. Davis[3], Peter Fawdon[1], Peter M. Grindrod[3], John C. Bridges[4], Elliot Sefton-Nash[5], and Rebecca M. E. Williams[6]

[1]School of Physical Sciences, The Open University, Milton Keynes, UK, [2]Department of Earth Sciences and Engineering, Imperial College London, London, UK, [3]Department of Earth Sciences, Natural History Museum, London, UK, [4]Space Research Centre, School of Physics and Astronomy, University of Leicester, Leicester, UK, [5]European Space Research and Technology Centre, Noordwijk, Netherlands, [6]Planetary Science Institute, Tucson, AZ, USA

Abstract A major debate in Mars science is the nature of the early Mars climate, and the availability of precipitation and runoff. Observations of relict erosional valley networks have been proposed as evidence for extensive surface runoff around the Noachian-Hesperian boundary. However, these valley networks only provide a time-integrated record of landscape evolution, and thus, the timing, relative timescales and intensity of aqueous activity required to erode the valleys remain unknown. Here, we investigate an ancient fluvial sedimentary system in western Arabia Terra, now preserved in positive relief. This ridge, "Aram Dorsum," is flat-topped, branching, ~85 km long, and particularly well preserved. We show that Aram Dorsum was an aggradational alluvial system and that the existing ridge was once a large river channel belt set in extensive flood plains, many of which are still preserved. Smaller, palaeochannel belts feed the main system; their setting and network pattern suggest a distributed source of water. The alluvial succession is up to 60 m thick, suggesting a formation time of 10^5 to 10^7 years by analogy to Earth. Our observations are consistent with Aram Dorsum having formed by long-lived flows of water, sourced both locally, and regionally as part of a wider alluvial system in Arabia Terra. This suggests frequent or seasonal precipitation as the source of water. Correlating our observations with previous regional-scale mapping shows that Aram Dorsum formed in the mid-Noachian. Aram Dorsum is one of the oldest fluvial systems described on Mars and indicates climatic conditions that sustained surface river flows on early Mars.

Plain Language Summary The oldest regions of Mars contain ancient valleys, carved by running water, and sinuous ridges, often interpreted as the remnants of former riverbeds, left upstanding by erosion. These "inverted channel" systems provide insight into Mars's ancient climate and hydrologic cycle. We use high-resolution satellite images to investigate "Aram Dorsum," an 85 km long ridge system in the Arabia Terra region. Our observations show that Aram Dorsum is composed of sedimentary rocks, originally deposited in rivers or their adjacent floodplains. The Aram Dorsum sedimentary material is up to 60 m thick, which, by comparison with similar sedimentary deposits on Earth, suggests that the Aram Dorsum river system was active for between 10,000 and 10 million years. Our study also indicates that Aram Dorsum was formed around 3.9 billion years ago, an age consistent with other evidence for ancient rivers and lakes in this region. The water that flowed within the rivers at Aram Dorsum probably came from both locally and regionally generated rainfall or snowfall, rather than a single point source of water, such as large distant ice sheets. Our observations therefore point to an ancient Martian climate that supported precipitation and river flow for thousands or millions of years.

1. Introduction

Numerous Noachian-aged terrains on Mars are dissected by systems of valleys incised into bedrock and are interpreted to have formed by fluvial erosion (e.g., Carr, 1987; Craddock & Howard, 2002; Hynek Beach & Hoke, 2010; Hynek & Phillips, 2001; Irwin & Howard, 2002). These fluvial systems are some of the strongest evidence for ancient surface runoff, probably caused by precipitation or snowmelt (e.g., Craddock & Howard, 2002). Valley networks commonly enter and exit impact craters and depressions suggesting that these were topographic lows that infilled with water forming palaeolake basins (e.g., Fassett & Head, 2008a; Goudge et al., 2016). Moreover, many valley networks terminate in sedimentary fan

Resources: Joel M. Davis, Peter Fawdon, Elliot Sefton-Nash
Software: Elliot Sefton-Nash
Supervision: Matthew R. Balme
Visualization: Matthew R. Balme, Peter Fawdon
Writing - original draft: Matthew R. Balme, Sanjeev Gupta, Joel M. Davis, Peter Fawdon
Writing – review & editing: Matthew R. Balme, Sanjeev Gupta, Joel M. Davis, Peter Fawdon, Peter M. Grindrod, John C. Bridges, Rebecca M. E. Williams

deposits, interpreted as both alluvial and delta fans (e.g., Di Achille & Hynek, 2010; Fawdon et al., 2018; Goudge et al., 2017; Kraal et al., 2008; Malin & Edgett, 2003; Moore et al., 2003; Moore & Howard, 2005; Rice et al., 2013). Morphometric analysis of these fluvial systems suggests that the majority probably formed during the late Noachian (Hoke et al., 2011) or late Noachian to early Hesperian (e.g., Fassett & Head, 2008b; Howard et al., 2005; Irwin, Craddock, & Howard, 2005), in an arid to semiarid climate (e.g., Ramirez & Craddock, 2018), possibly supported by a multibar CO_2 atmosphere (e.g., Jakosky et al., 2017). An alternative interpretation is that the climate was colder and dryer and that valley networks formed due to infrequent melting of large ice sheets occupying the southern highlands (e.g., Fastook & Head, 2015; Palumbo et al., 2018; Wordsworth et al., 2015).

Although the distribution and geomorphology of the valley networks have previously been investigated (e.g., Di Achille & Hynek, 2010; Howard et al., 2005; Irwin, Howard, et al., 2005), these landforms only provide a record of time-integrated landscape erosion; it is difficult to extract the temporal history of surface processes. On Earth, geologists use the sedimentary record to reconstruct the temporal evolution of surface environments. However, there have been relatively few investigations of depositional fluvial systems on Mars, by virtue that progressive accumulation and burial of sediment makes it challenging to decipher these systems from satellite plan view observations. Although the aggradation of sediment records a more complete picture of the early Mars environment, cross sections or erosional windows are required to interrogate this part of the geological record. For example, fluvial sedimentary rocks have also been observed in situ on the Martian surface using the National Aeronautics and Space Administration's Mars Science Laboratory Rover. Observations of fluvial conglomerates (Williams et al., 2013) and detailed analysis of grain size, texture, and geometry of sedimentary structures in sandstone outcrops at the Shaler and Kimberley outcrops (e.g., Edgar et al., 2018; Grotzinger et al., 2015) provide robust evidence for fluvial activity ~3.5 billion years ago in Gale crater. However, Gale crater only provides a record of Hesperian Mars and does not tell us about Mars' earliest fluvial activity.

Davis et al. (2019, 2016) presented evidence for an extensive network of Noachian age depositional fluvial channel belts, now exposed in inverted relief, within erosional windows in the Arabia Terra region. These fluvial systems, and others previously described in the Aeolis Dorsa region (e.g., Burr et al., 2010; Cardenas et al., 2018; Di Pietro et al., 2018; DiBiase et al., 2013; Hughes et al., 2019; Kite et al., 2015; Williams et al., 2013), are consistent with formation by self-formed channels in an aggradational alluvial environment (Davis et al., 2019, 2016). Although many of the sinuous ridges that define these inverted channels are discontinuous and heavily eroded, a few examples are well preserved and have sufficient exposure for detailed analysis with orbital remote sensing data. One such example is Aram Dorsum, a kilometer wide, ~85 km long, sinuous, branching, flat-topped ridge in Western Arabia Terra (Figure 1). Aram Dorsum was shortlisted as a landing site for ExoMars *Rosalind Franklin* Rover (Vago et al., 2017) and was ranked third in the final landing site choice.

In this study, we (i) characterize the paleogeomorphology of the Aram Dorsum ridge system and related rock outcrops, (ii) establish its stratigraphic context to determine when it was emplaced, and (iii) reconstruct the depositional environment in which it formed. From this, we discuss what the existence of Aram Dorsum and similar inverted channel belts in Arabia Terra mean for the Martian climate during the time these features were emplaced. Note that when we refer to "Aram Dorsum," we refer only to the ridge system itself, but when we refer to the "Aram Dorsum study area," we refer to the extent shown in Figure 1d.

2. Geographic and Stratigraphic Setting of the Aram Dorsum Study Area

Arabia Terra is a region of predominantly Noachian age (as mapped by Tanaka et al., 2014) cratered terrain located between Mars's fluvially dissected southern highlands and the younger surface of the northern lowlands (Figure 1a). Extending ~5,000 km east-west by ~2,000 km north-south, Arabia Terra is relatively low-lying compared to the highland terrain that lies to its south and is of a comparable age, dropping in elevation by only about a kilometer across its western north-south extent. The Aram Dorsum study area encompasses a shallow (~200–300 m of relief) depression in heavily cratered terrain in the west of Arabia Terra (Figure 1c). The study area (Figure 1d) is within terrain mapped as *Middle Noachian Highland unit* in the global-scale Mars geological map (Tanaka et al., 2014) or in terrain mapped as mid- to late-Noachian age *Lower etched unit*, in more recent, larger-scale geological mapping (Hynek & Di

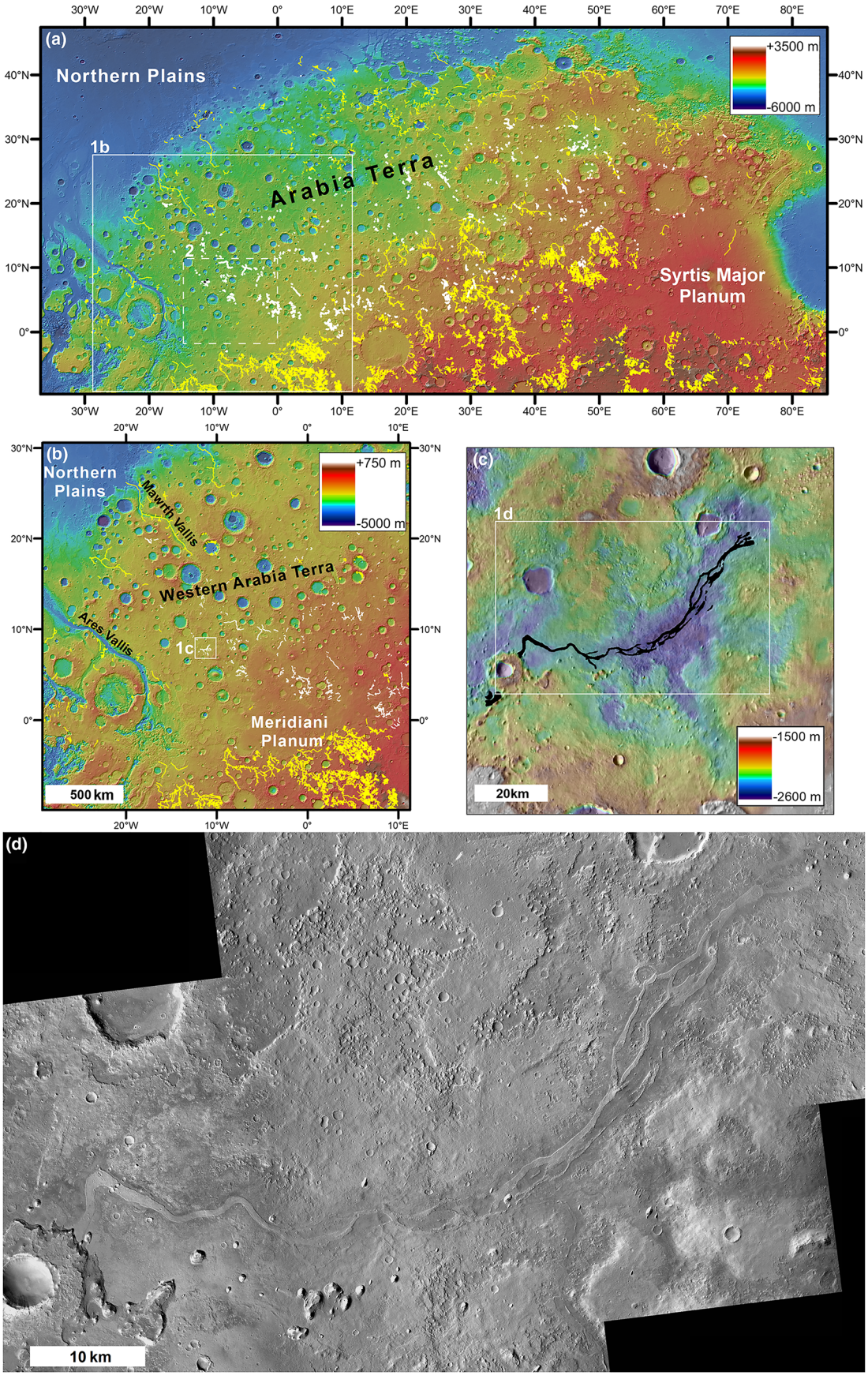
(a)
Northern Plains
Arabia Terra
Syrtis Major Planum
1b
2
+3500 m
-6000 m
(b)
Northern Plains
Mawrth Vallis
Western Arabia Terra
Ares Vallis
1c
Meridiani Planum
+750 m
-5000 m
500 km
(c)
1d
-1500 m
-2600 m
20km
(d)
10 km

Achille, 2017). In both of these morphostratigraphic mapping efforts, which used 100 m per pixel scale infrared-wavelength image data, the stratigraphically lowest and oldest units in Western Arabia Terra are early- to mid-Noachian in age have rugged surface expression of topography, contain many degraded craters, and show examples of layered, apparently sedimentary, materials. These units are interpreted to comprise a mixture of impact, volcanic, fluvial, and basin materials that were heavily degraded and, in places, tectonically deformed (Hynek & Di Achille, 2017; Tanaka et al., 2014).

Overlying the oldest, heavily cratered materials in Western Arabia Terra are subhorizontally layered, sedimentary units (Figure 2) that are up to hundreds of meters thick, referred to either as the "Etched Terrain" units or the Arabia Terra "mantling unit" (e.g., Edgett, 2005; Fassett & Head, 2007; Moore, 1990). The Etched Terrains contain distinctive sulfate spectral signatures (Arvidson, 2005) indicative of aqueous alteration in a low-pH environment (Bibring, 2006). The Etched Terrains show extensive morphological evidence for erosion, such as pits, steep, niche-indented scarps, and outliers. The terrain becomes progressively more eroded to the north and east. Numerous erosional inliers expose older Noachian terrains throughout the region. The friable Etched Terrain units conform to the gentle underlying south-north slope (Hynek & Phillips, 2008), and outliers are often found within topographic lows, showing both that the Etched Terrains were once more extensive and also that they overly the subjacent, heavily cratered units unconformably. Based on impact crater size frequency statistics, the Etched Terrains have been determined to be late Noachian/early Hesperian in age (Hynek Beach & Hoke, 2010; Hynek & Di Achille, 2017; Hynek & Phillips, 2008; Zabrusky et al., 2012). Most of the erosion that has reduced the volume of the Etched Terrains appears to have occurred within the tens or few hundreds of millions of years since their deposition, possibly by eolian abrasion and deflation (Zabrusky et al., 2012). Proposed origins for the Etched Terrains include deposition by volcaniclastic or eolian processes, perhaps combined with deposition of evaporites in shallow, groundwater-fed lakes (e.g., Andrews-Hanna et al., 2010; Hynek & Phillips, 2008).

In southwest Arabia Terra, the Noachian-early Hesperian-age regional stratigraphy is overlain by hematite-bearing, Hesperian-age deposits in Meridiani Planum (Hynek & Phillips, 2008). These are interpreted to have formed by a combination of eolian and evaporitic processes, and later alteration by groundwater (Grotzinger et al., 2005; Squyres & Knoll, 2005). The extensive sedimentary deposits of Meridiani Planum and the Etched Terrains together unconformably overlie the older, heavily cratered Noachian units. Importantly, at their southernmost extent, these younger sedimentary units superpose the valley networks that are incised into early- or mid- Noachian cratered units, such that few fluvial valley systems are exposed in southwest Arabia Terra (e.g., Hynek Beach & Hoke, 2010; Figure 1a). This superposition stratigraphic relationship constrains the age of incision of the valley networks in this region to have occurred during or prior to the early-Hesperian, when the Hematite unit was emplaced (Hynek & Di Achille, 2017).

3. Data and Methods

3.1. Data

The Aram Dorsum study area (Figure 1) was characterized using a variety of imaging, surface temperature, and topographic datasets. The data were ingested into ArcGIS software for analysis and, when necessary, processed in ISIS3 software. The main datasets used in this study are CTX images, HiRISE images (High Resolution Imaging Science Experiment; 25 cm per pixel; McEwen et al., 2007), MOLA altimetry data (Smith et al., 2001), and nighttime and daytime THEMIS images (THermal EMission Imaging Spectrometer; 100 m per pixel; Christensen et al., 2001). From these data, other derived products were created, including HiRISE stereo digital elevation models (DEMs) and CTX stereo DEMs, produced

Figure 1. (a) MOLA topographic map of the Arabia Terra region of Mars. Warmer colors show topographic highs, cooler colors show topographic lows. Yellow lines are the locations of valley networks (Hynek & Di Achille, 2017); white lines are locations of inverted channels in Arabia Terra (Davis et al., 2016). Solid white box shows location of (b). Dashed white box shows the location of Figure 2. (b) MOLA topographic map (again, warmer colors show topographic highs, cooler colors show topographic lows) showing the location of the Aram Dorsum study area (white box) within Western Arabia Terra. Yellow lines are the locations of valley networks (Hynek & Di Achille, 2017); white lines are locations of inverted channels in Arabia Terra (Davis et al., 2016). White box shows location of (c). Note the color "stretch"on the MOLA map is different to (a) to emphasize the topography. (c) Local MOLA topographic context of the Aram Dorsum main ridge system, shown as the bold black line. White box shows location of (d). (d) CTX (ConTeXt imager; 6 m per pixel; Malin et al., 2007) mosaic showing Aram Dorsum. North is toward the top of the image in this and all other images unless otherwise stated. Lighting is from the western direction in this and all images unless otherwise stated. MOLA credit NASA/JPL/GSFC. CTX image credit NASA/JPL/MSSS.

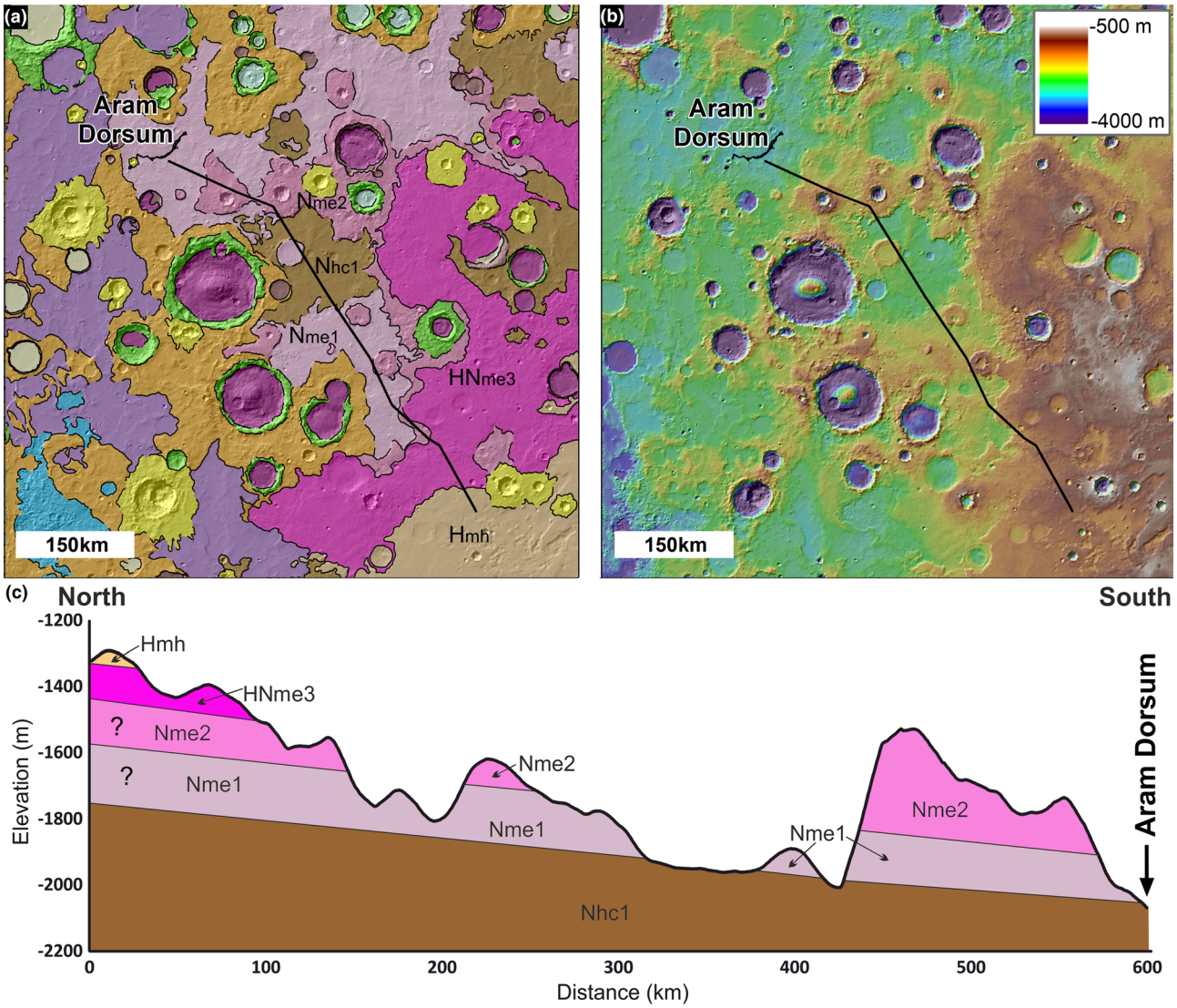

Figure 2. Geographic and stratigraphic context of Aram Dorsum. (a) Part of Terra Meridiani region geological map (Hynek & Di Achille, 2017). Dark line shows south to north profile. Main units as shown in (c). The main Aram Dorsum ridge is shown in the upper left (dark line). (b) MOLA topography of the same region. (c) Highly simplified cross section from south to north. Unit names as per Hynek and Di Achille (2017): Nhc1 is the "Subdued crater unit" (early to middle Noachian), Nme1 and Nme2 are "lower and middle Etched units" (middle to late Noachian), HNme3 is "upper Etched unit" (late Noachian/early Hesperian), and Hmh is "Hematite unit" (early Hesperian). Note the uncertainty as to whether lower etched unit continues under upper etched units or instead pinch-out further north. Note also the uncertainty, as illustrated in the cross section, about whether Aram Dorsum sits within Nhc1, or NMe1. This is discussed further in section 4.3. Map credit Hynek and Di Achille (2017) and USGS. MOLA data image credit: NASA/JPL/GSFC.

following the method of Kirk et al. (2008) with a horizontal spacing of 1 and 20 m per pixel, respectively. Other data sets used to a more minor extent include High-Resolution Stereo Camera; Neukum & Jaumann, 2004) images and DEMs (up to 50 m per pixel; Jaumann et al., 2007). A list of specific images used is provided (supporting information Table S1). Multispectral and hyperspectral remote sensing data sets such as OMEGA (Bibring et al., 2004) and CRISM (Murchie et al., 2007) were not used in this study, as almost all such observations were noisy and provided no clear signatures. We infer that the poor quality of the spectral data in the region is due to the surface having a dust cover (perhaps only submillimeter in thickness) that prevents collection of any clear compositional information.

3.2. Approach to Mapping

To characterize the local stratigraphy and determine the formation mechanisms and possible depositional environments represented by the key stratigraphic units in the Aram Dorsum region, we constructed a

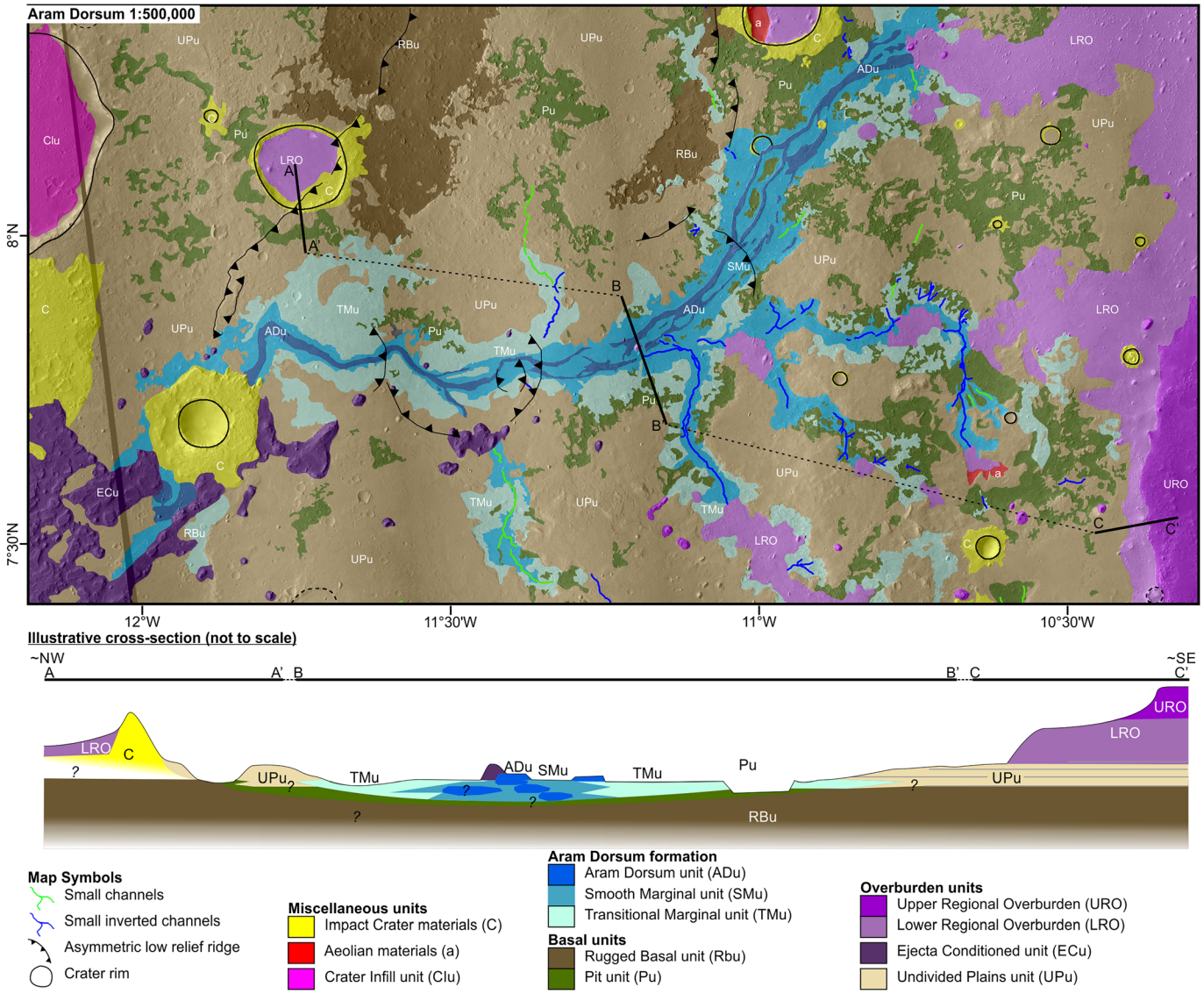

Figure 3. Morphostratigraphic map of the study area (top). Map units are described briefly in the text and more fully in supplementary online materials. The cross section (bottom) illustrates the inferred stratigraphy in the direction from NW (left) to SE (right), and only shows key segments (bold lines on map) that best represent the stratigraphy of the entire system, rather than being an accurate depiction of the topography and thicknesses of each unit. The cross section is not to scale.

morphostratigraphic map of the study area (Figure 3). Our main focus was on determining the relationships between the sinuous ridge segments, which comprise Aram Dorsum, smooth plains associated with the ridge, and the surrounding terrains. Mapping used a mosaicked base layer of CTX images (supporting information Text S1). Areas of consistent texture, surface morphology, relief, and apparent albedo were mapped as units. Scarps, or breaks in slope, also provide information about contacts where units clearly superposed one another, as revealed by erosion. Thus units are defined as spatially extensive regions of similar surface morphology that are also inferred to be the surface expression of a rock body (or surficial materials) that was deposited in a consistent stratigraphic position relative to other units in the study area. Line work was created digitally using ArcGIS software at a scale of between 1:30,000 and 1:100,000. Figure 3 is shown at a scale of ~1:500,000. In addition to the CTX base layer, HiRISE data and THEMIS data were used to determine the meter-scale surface morphology and the thermophysical properties of the units respectively. These data provided further clarification and helped determine unit boundaries, but, in general, the map represents our interpretations of the study area based mainly on the similarities and

Table 1
Crater Size Frequency Data for Selected Units in the Study Area

Unit	N. craters counted	Area ($\times 10^2$ km^2)	Size range fitted (km)	No. craters in fitted range	Crater retention model age (Ga)
Aram Dorsum (*ADu*)	283	0.31	0.08–0.2	21	0.22 (+0.05, −0.05)
Local overburden (*UPu*) NW area	1417	10.9	0.6–3	39	3.74 (+0.03, −0.03)
Local overburden (*UPu*) S area	1228	17	0.5–3	41	3.47 (+0.05, −0.08)
Local overburden (*UPu*) NE area	1747	5.8	0.35–3	104	3.64 (+0.02, −0.02)
Regional basement area	213	460	2.5–80	65	3.91 (+0.02–0.02)

Note. These data are shown graphically in Figure 13.

differences in the CTX-scale morphology and relief of the study area, combined with inference about stratigraphic relationships drawn from outcrop pattern and relief.

3.3. Impact Crater Counting

To estimate emplacement ages for some of the mapped surfaces, we employed impact crater size frequency statistics. We identified impact craters in CTX images or HiRISE images and digitized them in ArcGIS using the three-point method in the CraterTools software package (Kneissl et al., 2011), guided by the methodologies of Platz et al. (2013) and Tanaka et al. (2014). When estimating emplacement ages vs. exposure ages, we employed various approaches to counting craters and the minimum size of crater identified depended on the specific study area. For crater counts in the basement units, all larger craters were counted, including those with evidence of infilling by later materials. To estimate the exposure age of units, we selectively counted only those crater that appeared to have not been exhumed, looking for evidence such as fresh and upstanding crater rims, blocky rubble in the proximal ejecta, no material infilling the crater floor, and no evidence for any later deposits overlying the rims.

To determine crater retention model ages, we used the CraterStats software package (Michael & Neukum, 2010). We considered the whole cumulative population and then fitted ages using the Hartmann (2005) production function and chronology. To interpret model ages we used the parts of the size frequency distributions that best fitted isochrons—often this is from a restricted part of the size range of the data set and is shown in Table 1 in section 4.3. Smaller crater in particular are often "lost" due to erosion or burial. Additionally, we discuss the validity of our results using crater count-derived model ages made using areas <1,000 km^2 (Warner et al., 2015) as well as potential interpretation caveats associated with burial and erosion.

4. Mapping and Observations

4.1. Morphostratigraphic Map Units and their Interpretation

Figure 3 shows the morphostratigraphic map and an inferred schematic cross section of the study area around Aram Dorsum. We provide only brief unit descriptions and interpretations here, but include illustrative figures and fuller description of map units in supporting information section S1. Top level map unit interpretations are included to provide context for the observations presented in sections 4.2 and 4.3. Unit names are given as morphological or contextual descriptions only. The units are put into a regional chronostratigraphic framework in section 4.3. We group the units into (i) the *Aram Dorsum formation*, which includes units that make up the Aram Dorsum ridge and materials interpreted to have been deposited at the same time and in association with it; (ii) the Basal units, which includes units inferred to stratigraphically underlie the Aram Dorsum formation; and (iii) the Overburden units, which includes units inferred to stratigraphically overlie the Aram Dorsum formation (both regionally extensive overburden units and local-scale overburden units). Except for the Aram Dorsum formation, we do not suggest that these are formal geological "groups" in the sense that they are assemblages of formations; we have simply grouped the units by their stratigraphic position.

4.1.1. Study Area Physiography and Tectonics

Description: The study area is an approximately 100 by 30 km topographic low (Figures 1–3) nestled between several 50–100 km diameter impact craters in Arabia Terra. The study area has only 300–400 m of relief, created mainly by a large topographic step at the eastern part of the study area. Aram Dorsum sensu

stricto itself is a flat-topped, steep-sided, sinuous ridge, which is oriented SW-NE (Figure 1c). Other more subtle topographic features in the study area include N-S trending linear topographic rises, and low topographic rises or subtle scarps forming circular or arcuate patterns. In the eastern part of the study area, areas of Etched Terrain (Lower Regional Overburden, LRO, and Upper Regional Overburden, URO in Figure 3) appear to overlie Aram Dorsum.

Interpretation: We interpret the area hosting the Aram Dorsum ridge as an erosional window (an inlier) through the extensive local and regional overburden units that presently surround it. The boundaries of the inlier form distinct scarps. We interpret the other subtle topographic features to be reverse-fault-controlled "wrinkle ridges" and the expressions of ancient, buried impact craters (Figure 3).

4.1.2. Basal Units

Description: The oldest observable part of the stratigraphy consist of units characterized by rugged surfaces and are mapped as morphostratigraphic unit "RBu." These units were identified based on observations of surface textures in CTX images. RBu is exposed at the base of large erosional windows through the local superposing materials and/or materials in the Aram Dorsum formation. These surfaces have moderate brightness in THEMIS nighttime IR images.

Pit units (Pu) comprise a population of ~1–10 km wide, flat-bottomed, erosional pits that occur within both Aram Dorsum formation (section 4.1.3) and local overburden units (section 4.1.4). They appear to represent surfaces exposed from beneath these units. The pits floors are generally of low albedo, are smooth at 10–100 m scale, contain remnant outliers of the units in which they form, and are moderate bright in THEMIS nighttime IR image so are distinct from the Rugged Basal unit surface textures. Pu commonly contains polygonal fractures with a distinctive "Wide-Fracture" morphology (see section 4.2.4). This "Wide-Fractured" surface is erosion resistant compared to the materials in which the pits occur, as it seems to form a barrier to further erosion. Where the Pit unit wide-fractured surface *has* been eroded, the material beneath is rugged and similar in appearance to the RBu basal unit. These pits appear only to form spatially close to Aram Dorsum or one of its subsidiary ridges.

Interpretation: These morphostratigraphic units appear to have been exposed by erosion and removal of overlying material. RBu units are the oldest terrains in the study area. We interpret the contact between the basal unit and overlying strata to probably be unconformable: a few kilometer-scale craters within RBu appear to be overlain by overlying material, demonstrating a time gap between emplacements. We interpret the current exposed RBu surface as an exhumed palaeosurface that was heavily modified by impact cratering and other processes, though it is unclear how significantly the RBu materials have been modified since emplacement, burial, and reexposure. We do not imply that RBu units are true "crystaline basement" or that they represent a specific body of rock, only that they are terrains with consistent morphology that are superposed by all other units in the study area.

The Pit units have a distinctive surface texture and setting but are clearly of competent material rather than loose infill. They appear to form a laterally extensive, but relatively thin, rock body (or bodies) stratigraphically immediately below the Aram Dorsum formation (section 4.1.3) but stratigraphically above the RBu basal unit. The Pu surface is only exposed where erosion allows. It is unknown whether Pu materials represent a preexisting unit (or units) emplaced upon RBu, prior to Aram Dorsum formation or whether it was deposited as the first subunit within the Aram Dorsum formation (section 4.1.3). The origin of this unit is discussed more in section 5.1.

We interpret Pu materials to be stratigraphically above the basal material but stratigraphically (and topographically) below and in contact with the Aram Dorsum marginal units. Pu could therefore be placed within the Aram Dorsum formation or grouped with the basal units.

4.1.3. Aram Dorsum Ridge and Marginal Units (the *Aram Dorsum Formation*)

Description: Strata comprising the Aram Dorsum ridge and spatially associated marginal units are exposed within the topographic low that runs approximately east to west though the center of the study area. This group of units includes the multiple threads of the Aram Dorsum ridge itself (Aram Dorsum unit; ADu), the smooth marginal materials found adjacent to the ridge (Smooth Marginal unit; SMu), and the Transitional Marginal unit, TMu, found adjacent to the SMu. Together, these units comprise the *Aram Dorsum formation*, as our observations suggest that they are closely related stratigraphically and physically and have lithological similarities between each other.

The ADu is a flat-topped, sinuous ridge, sometimes with multiple branches, that ranges in width from ~300 m to ~1.5 km. The ridge mean width, measured for the largest branch, sampled every 10 km, is 700 m. The Aram Dorsum ridge has moderate to low thermal inertia relative to the other units in the study area, based on its middle- to dark-toned appearance in nighttime THEMIS images. A branching system of narrower subsidiary ridges join the main Aram Dorsum ridge. Sometimes these subsidiary forms are troughs or channels, rather than ridges. They are recorded as line features on the map (Figure 3). The morphology of the Aram Dorsum ridge system and its subsidiary ridges are described in more detail in sections 4.2.1 and 4.2.2.

The SMu surrounds Aram Dorsum and many of the subsidiary ridges. The unit forms low relief terrain and has a smooth texture in both CTX and HiRISE images. It is characteristically bright in THEMIS nightime data, suggesting it is of high relative thermal inertia. Where SMu meets Aram Dorsum (i.e., at an "inner"-contact), the SMu is generally superposed by the Aram Dorsum unit, but in some places the two units show transitional relationship (see section 4.2.1).

Away from Aram Dorsum, SMu grades into a similar unit, TMu, that appears similar, but more rugged and of more moderate brightness in THEMIS nighttime images. Where either SMu or TMu meet other units (other than ADu), the units are superposed by plains-forming materials (see section 4.1.4). HiRISE images reveal that the TMu consists of broken up, rugged outliers of plains materials superposing the SMu. Thus, the TMu is not a morphostratigraphic unit in the strict sense, but it instead in plan view is formed of a mixture of SMu textures and remnant superposing materials (mainly the Undivided Plains unit, UPu described in section 4.1.4) to various degrees. We include TMu as a separate map unit mainly because it is too extensive to represent as a gradational contact line feature. TMu and SMu are therefore equivalent in the local stratigraphy.

The Aram Dorsum formation materials superpose and locally bury ancient impact craters, as evidenced by partly buried degraded crater rims, and from the presence of circular relief patterns revealing the presence of "ghost craters" within the units.

Interpretation: We interpret Aram Dorsum and its subsidiary ridges to represent the inverted expression of a fluvial system, consistent with the interpretations of Davis et al. (2019, 2016). The continuity, planform shape, and flat top argue against it being a tectonic or lava flow feature. The ridge systems are preserved in positive relief because they are composed of material more resistant to erosion than the surrounding terrains. The relationship between the marginal units and the Aram Dorsum ridge is complex and is discussed in section 4.2.3.

4.1.4. Local Overburden Units

Description: Exposed north and south of Aram Dorsum are plains-forming units of variable surface roughness and relief that includes the Undivided Plains units (UPu) and Ejecta-conditioned Plains units (ECu).

The Undivided Plains units are moderate to smooth in appearance at CTX scale and contain a moderate number of impact craters. South of Aram Dorsum, the Undivided Plains unit is moderate to dark in THEMIS nighttime data, suggesting a relatively low thermal inertia, and is perhaps radially distributed with respect to an ~30 km diameter crater just south of the study area (the rim is just visible at the bottom of Figure 1c). North of Aram Dorsum, the unit is slightly brighter in nighttime THEMIS data and contains more impact craters. The Undivided Plains unit probably consists of several subunits based on observations of discontinuous internal scarps and boundaries. However, all these subunits appear to occupy a consistent stratigraphic position, so further dividing it seems unnecessary for this study.

The Ejecta-conditioned Plains unit, ECu, unconformably overlies both the Undivided Plains unit (this is shown by outliers of ECu within an impact crater in the Undivided Plains unit) and the Aram Dorsum/Aram Dorsum marginal units. It is continuous in the southwestern part of the study area, but forms linear chains of erosional outliers toward the middle of the study area. The distribution of these outliers suggests that they are related to an ~50 km diameter impact crater southwest of the study area.

Interpretation: These Plains units are interpreted as overburden materials of generally unknown origin. The spatial extent of UPu suggests it might be composed mainly of ejecta materials from local and regional impact craters. ECu materials could be either continuous ejecta from a crater to the south west of the study area, or materials of unknown origin conditioned or protected by a thin ejecta layer associated with this crater.

4.1.5. Regional Overburden Units

Description: The eastern part of the study area is dominated by two-layered, cliff-forming units, each up to several hundred meters thick. These are of regional extent and are termed the Upper Regional Overburden (URO) and LRO units. They are the youngest major units in the study area and include outliers, which crop out across the study area. Examples of outliers are observed both infilling impact craters and topographically low regions, and as small (km-scale laterally), ~50–100 m high, flat-topped or cone-shaped hills or mounds overlying the local overburden units or the Aram Dorsum units. Some outliers are tens of kilometers away from the main units, and others straddle stratigraphically lower unit boundaries, suggesting they were emplaced unconformably onto a (probably erosional) palaeosurface. The regional overburden units themselves have undergone significant erosion, as shown by the presence of erosional pits, scarps, and yardangs. The LRO unit is very bright in nighttime THEMIS images, whereas the URO unit is midtoned. The majority of the regional overburden outliers are bright in nighttime THEMIS, suggesting that they formed from the LRO unit.

Interpretation: Spatially, the regional overburden units correspond to the "Etched Terrain" units (Edgett, 2005; Hynek & Di Achille, 2017; Hynek & Phillips, 2008) that occur across western Arabia Terra and were presumably once far more spatially extensive. Given that an extensive outlier of the LRO unit is found within a crater in the northwest of the study area, we suggest that almost all of the study area was once buried by this material, probably to depths of at least ~100 m, given the heights of the overburden outliers in the study area. The erosional morphologies (e.g., yardangs) and the infilling of topographic lows by outliers of the LRO, suggest that wind erosion was (at least recently) a key process in the erasure of these units from across the study area.

4.1.6. Other Units

In addition to the major units described above, the map contains other units, unrelated to Aram Dorsum. These include impact ejecta and crater rims/floors, which are mapped if associated with discrete impact craters. Recent crater materials superpose other mapped units, although some appear also to have undergone significant erosion. There are also some small patches of recent surficial materials—mainly eolian Transverse Aeolian Ridges (e.g., Balme et al., 2008) and mass wasting deposits—but there are only a few areas large enough to be visible at the scale of Figure 3. Finally, in the west of the study region is an impact crater with a distinctively textured floor; this is labeled the Crater Infill unit.

4.2. Morphological Observations

4.2.1. Aram Dorsum Ridge

The Aram Dorsum ridge forms the most prominent morphological feature in the modern landscape in the study area. The ridge is linear to slightly sinuous in planform, comprising segments that form either a single thread or multiple threads combined to form a largely contiguous topographic feature (Figures 2 and 4). In the west, Aram Dorsum if formed from only a single ridge, but in the center and east of the map region it comprises up to five subparallel ridges in various states of degradation. Figure 4 shows also the locations of other images in this section. Aram Dorsum is exposed for a length of ~85 km and although parts of it are ~40 m tall above the adjacent flat-lying terrain, most of the ridge system has only 10–20 m of relief, and in places it is almost flush with the surrounding plains. The upper surface of the ridge has a smooth, flat top that retains craters, and sheds boulders, suggesting that it is composed of a resistant lithology. It is characterized by a distinct low thermal inertia. No structures such as stratification are apparent on the upper surface, though subtle curvilinear ridges and grooves lying parallel and subparallel to the ridge margins are present. There are also examples of polygonal fracturing of the flat surface of the ridge (see section 4.2.4). The margins of the ridge are generally steeper at the top than at their base and are generally well defined. In some segments, the margins comprise linear and smooth scarps, but in other segments the margins are heavily degraded with rubbly material at their base. The uppermost part of the ridge forms a distinct resistant capping layer, visible in HiRISE images, which is meter scale in thickness (Figure 5a). Beneath this uppermost resistant layer, few features are visible within the ridge flanks, although some clear examples of meter-scale layering are visible beneath the resistant capping layer (Figure 5b). An additional ~10–15 km of ridge flank exposure contain parallel striations that are consistent with layering, but meter-scale layering is generally either (i) fairly rare here or (ii) the exposure is too poor (due to burial or mass wasting) and/or the imaging quality is insufficient (due to shadowing, spatial resolution or noise) for the layering to be easily identified if present.

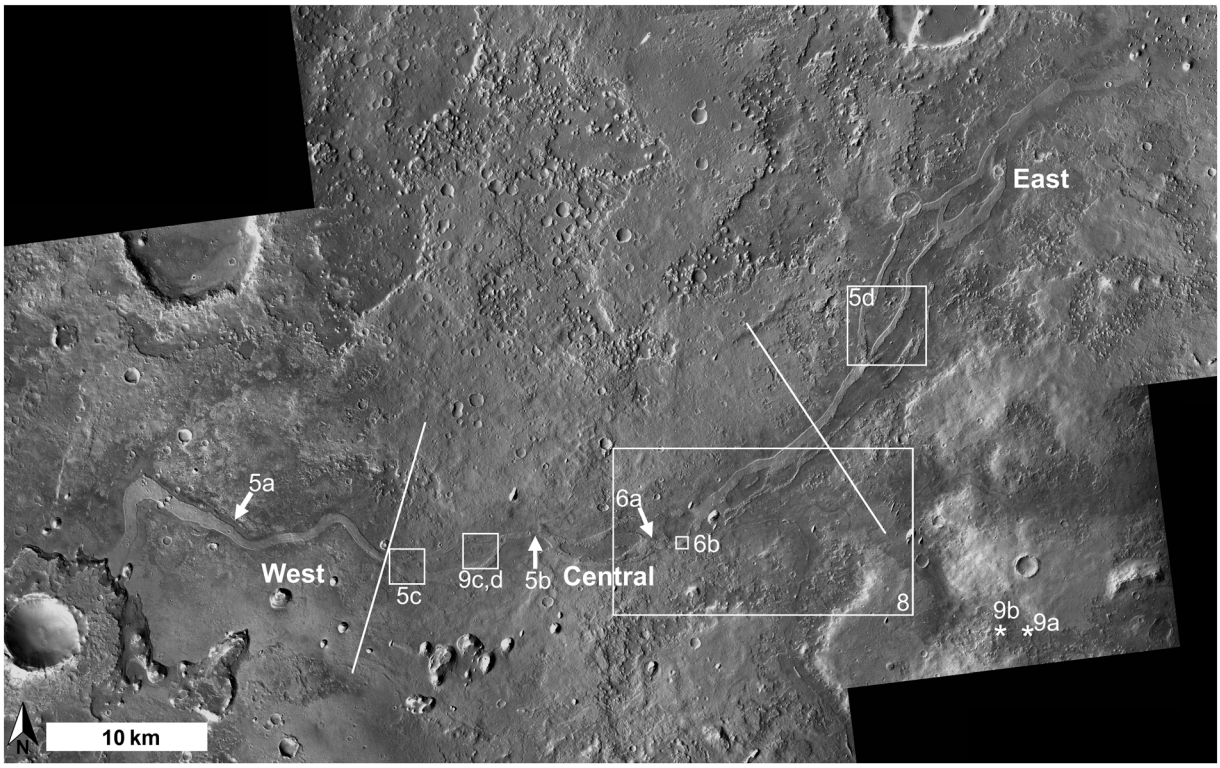

Figure 4. CTX mosaic showing the branching reforming planview morphology of Aram Dorsum in the eastern and central parts, transitioning to a single, sinuous morphology in the western part. Long white lines indicate the approximate separation between the western, central and eastern sections. This image also shows the locations of other figures (boxes show extents, arrows show viewpoint for oblique images, stars show image extents too small to be shown as boxes). Image credit NASA/JPL/MSSS.

The Aram Dorsum ridge shows marked variation in planform morphology along its ~85 km long length. The ridge widens along its length from ~500 m in the east to ~1,100 m across at its westernmost end, where it is buried by a 5 km diameter younger crater and its ejecta and by the ejecta-conditioned Plains unit. The eastern segment of the ridge has a NE-SW orientation and at its easternmost extent comprises shorter segments that may be single thread then branch into multiple contiguous strands that combine again to trace southwestward into a single thread. The branching and rejoining of individual strands appears to occur at a similar stratigraphic level in some examples (Figure 5c), but in others superposition relationships show older/younger ridges cross cutting one another, giving the impression of branching (Figure 5d) in lower-resolution images.

The central part of Aram Dorsum shows a change in orientation to more ENE-WSW, although it still has a planform characterized by branching and reconnecting ridge segments. Here, branches typically reconnect at apparently the same stratigraphic level (Figure 5c). The western third of the main ridge is oriented approximately E-W and is characterized by a single, well-defined, flat-topped ridge with a width of ~0.5–1.2 km. Here, the ridge planform shows several large-scale bends with wavelengths of ~5 km (Figure 2), with the westernmost bend showing pronounced sinuosity and a large ridge width. The mean sinuosity (i.e., along-ridge length divided by start-to-finish straight line length) of the whole system, based on 27 potential flow pathways, is 1.20, ranging between 1.19 and 1.21 depending on the pathway chosen, but the sinuosity of the western part alone is about 1.4.

There is evidence that the structure of Aram Dorsum is more complex than a single resistant layer "capping" a weaker layered substrate. Examples of resistant layers cropping out from within the ridge flanks can be seen in some places (Figure 6a) and vertically stacked ridge segments, each with a resistant upper layer, can also be seen (Figure 6b, and perhaps traces of this are seen in Figure 5c).

4.2.2. Subsidiary Ridge Networks Marginal to the Aram Dorsum Ridge System

Associated with the main Aram Dorsum ridge system, and inset within the SMu, are a series of up to eight narrow subsidiary sinuous ridges that are located on either side of the main ridge (Figures 7a–7c and

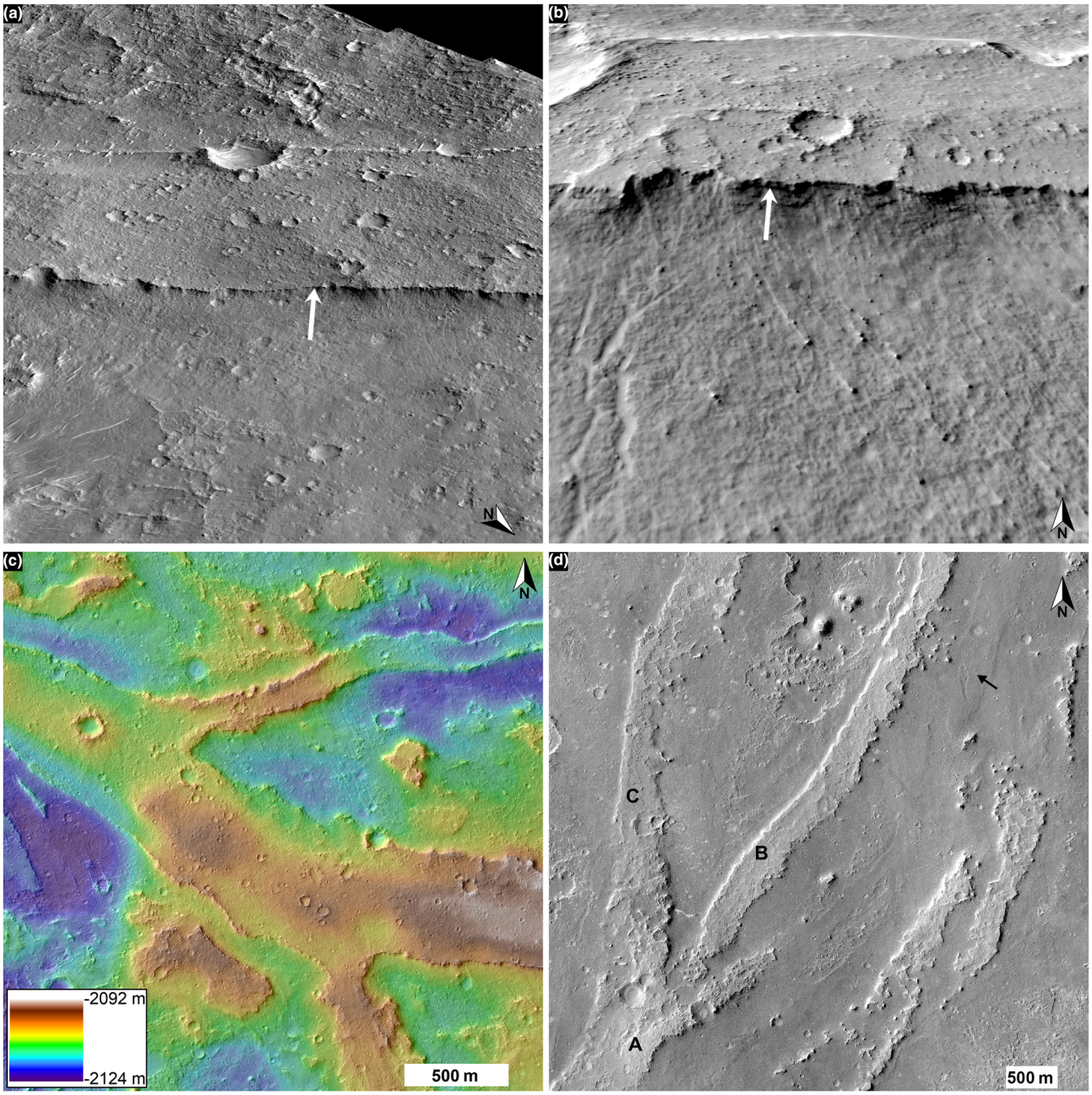

Figure 5. Examples of Aram Dorsum main trunk morphology as observable in HiRISE images and DEMs. (a) Oblique view looking southwest showing simple ridge morphology (~1 km long) in the western reach of Aram Dorsum. Note apparent erosion resistant unit "capping" the ridge (arrow). Vertical exaggeration is ×2. North is toward the bottom right. Illumination from the right. (b) Simple ridge morphology (~400 m long) in a branch of the central reach of Aram Dorsum. Note both the resistant upper-most layer and the apparently planar, subparallel bedding visible in the scarp below the top of the ridge. The ridge here is about 10 m high. Vertical exaggeration is ×2. North is toward the top. Illumination from the left. (c) Example of main trunk branching in the central reach of Aram Dorsum, in which the three branches all appear to join at the same stratigraphic level. Note the presence of what appears to be a subtle raised platform that follows the center line of the main ridge. HiRISE DEM overlain on HiRISE image. d) Evidence for vertical aggradation of channel bodies. Several Aram Dorsum channel ridges can be seen, set against the darker Smooth Marginal unit. Channel Branch "A" appears to superpose Branches B and C. In the east of the image, other channel body sections are visible. Arrowed is a faint lozenge-shaped mound that appears to be set within the smooth marginal materials. Other faint channel-like forms are also visible. All image credits NASA/JPL/UofA.

supporting information Table S2). These subsidiary ridges are subtle sinuous to curvilinear features, which join or at least approach the main Aram Dorsum ridge. The subsidiary forms are all much smaller than the main Aram Dorsum system, being only up to ~200 m in width at most, and with the longest example being less than 50 km long. All examples slope toward Aram Dorsum and have end-to-end mean gradients of

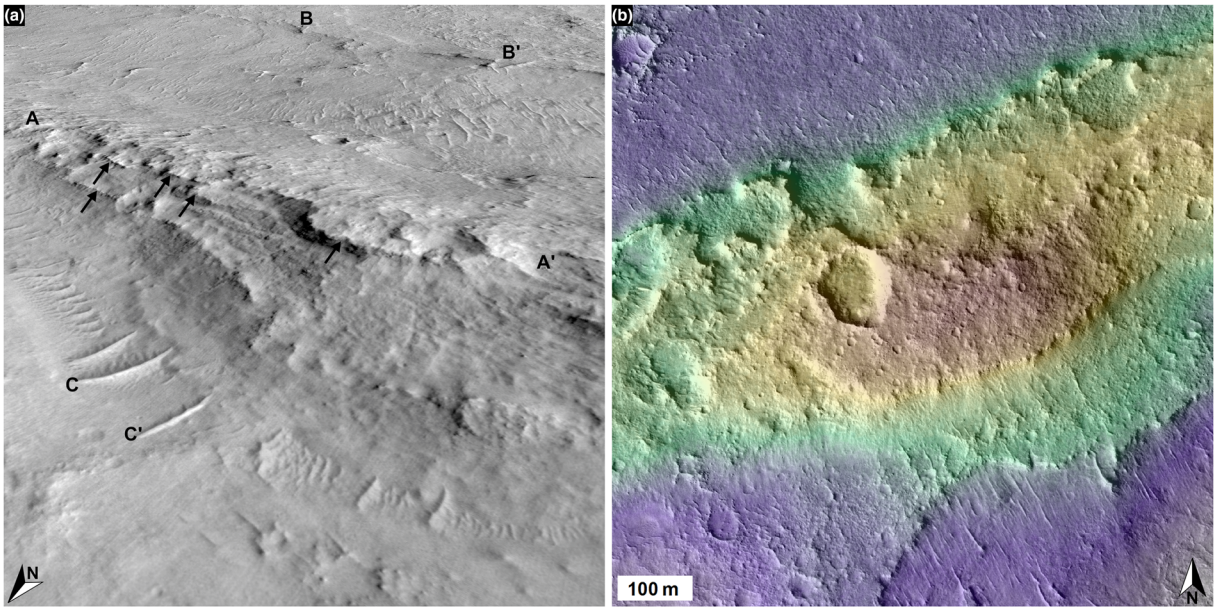

Figure 6. Examples of multiple resistant layers within Aram Dorsum. (a) Oblique view looking southeast showing the north side of a part of the Aram Dorsum main trunk ridge. Several resistant layers can be seen at the top of and within the ridge (arrows), cropping out at different heights within the flank. The line AA′ is along the ridge, BB′ in the distance marks the location of another section of the Aram Dorsum ridge complex. Distance BB′ is ~400 m, distance CC′ in the foreground is 35 m. The ridge section here is ~15 m high. Vertical exaggeration is ×2. Illumination is from the right. (b) Possible "stacked" channel bodies within the Aram Dorsum ridge. A central ridge, ~150 m wide, is set upon a wider (~400 m) platform-like flat-topped ridge. Both have steep margins, suggesting erosion resistance. Colors represent topography derived from a HiRISE stereo pair DEM (reds are highest, dark blues lowest). The central ridge is ~20 m high, and the lower ~10 m high. All image credits NASA/JPL/UofA.

<0.002–0.004. The elevation of parts of the subsidiary ridges most distant from Aram Dorsum ranges from −1950 to −2150 m; that is, from about the same elevation as Aram Dorsum for the shorter tributaries to about 200 m higher for the longer examples.

The subsidiary ridges networks are primarily stratigraphically enclosed within the SMu, although some examples occur in the local overburden unit, especially where this unit appears to be thin or discontinuous. Where the ridges occur in SMu, they generally have the same textures as the surrounding unit, and appear to be set within the materials that compose the unit. They may also be patterned with polygonal ridges or fractures, commonly found within this unit (see section 4.2.4).

Several of the subsidiary ridges show a complex morphology. They generally lack a flat top (with a few exceptions, such as Figure 7a), and commonly show a furrowed or pitted crest. There are also examples of negative relief channel-like forms, some of which transition from elongated or collinear pits into furrows (as observed elsewhere in Arabia Terra; Williams et al., 2017). The positive relief forms are in general more common (we have mapped ~150 km of subsidiary ridges and ~50 km of subsidiary channel-like forms) but are not usually capped by the resistant materials that define much of the main Aram Dorsum ridge. Examples of central ridges set on top of a low platform can be seen in Tributary 5 (Figure 7b), and there are also examples of lateral ridges and lineations running subparallel to the dominant tributary ridge. These morphologies might indicate the presence of resistant horizons within the ridge, but the small scale of the features and the extensive erosion makes it hard to identify these clearly.

The subsidiary ridge systems are typically approximately north-south oriented, which contrasts with the pronounced east-west orientation of the main Aram Dorsum ridge but sometimes show a less than 90° approach angle in the vicinity of Aram Dorsum. In particular, the southern branch of Subsidiary Ridge System 5 shows a marked 90° swing from its N-S orientation to the west within two kilometers of Aram Dorsum (Figure 8).

4.2.3. Marginal Units

The main Aram Dorsum ridge and its subsidiary elements overlie and are surrounded by flat-lying terrains from which they can be clearly distinguished in nighttime THEMIS data. In the CTX-based mapping we

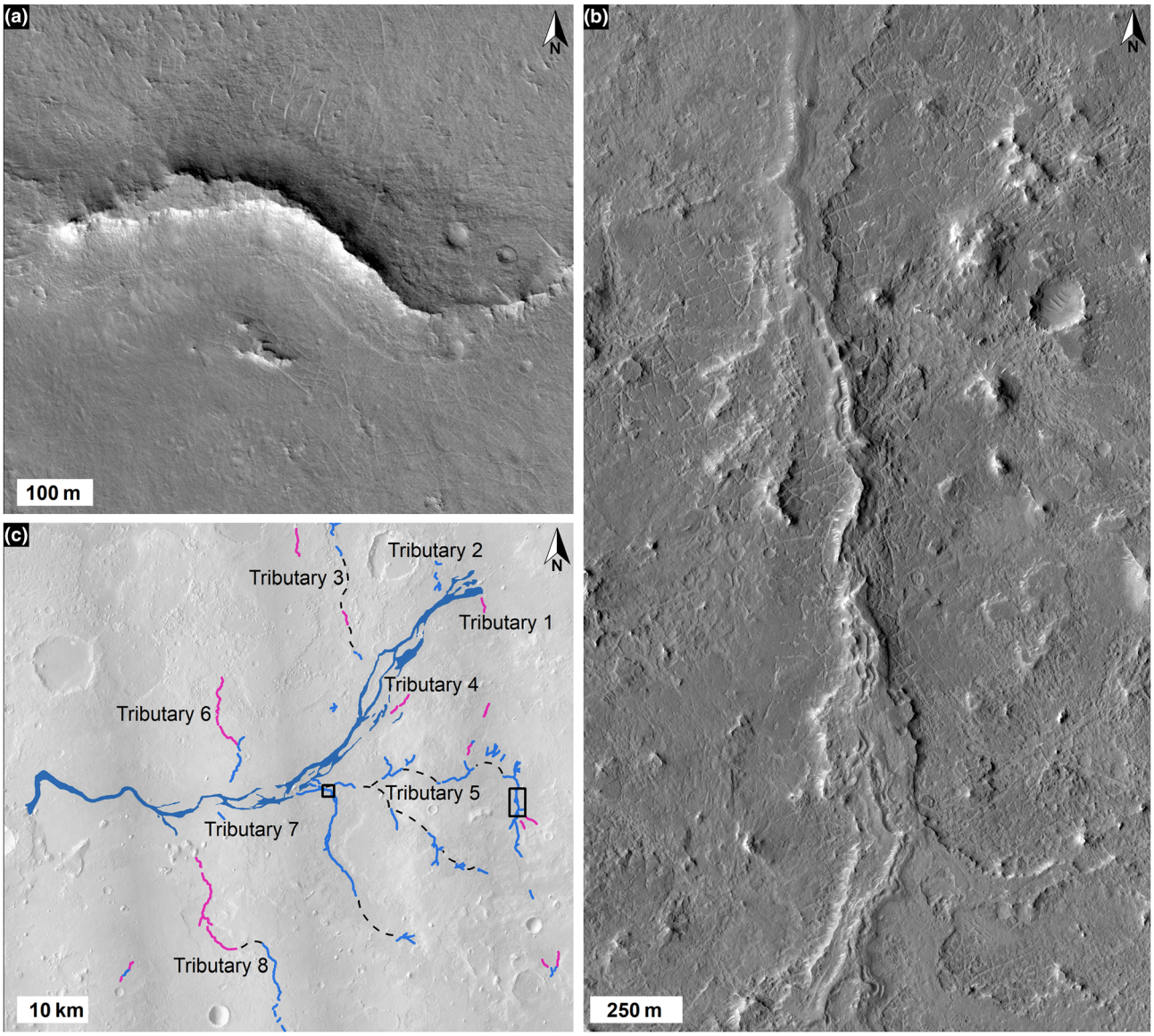

Figure 7. Tributary branches of Aram Dorsum. (a) Example of a small inverted channel belt with a resistant upper layer—similar to the Aram Dorsum main trunk. (b) Part of Tributary 5, in which the channel belt transitions from being a poorly defined ridge (without erosion resistant upper layer) set in Smooth Marginal unit deposits at the top of image, to more sharply defined ridge set on a low platform of Smooth Marginal unit materials. This low platforms has an edge defined by an erosional scarp with 'wide-fractured' style pits below it. Note also the more complex ridge-furrow form of the inverted channel here, especially in the lower half of the image. (c) Map showing tributary ridges and furrows/channels. At the center of the image is the Aram Dorsum main trunk system (dark blue). Smaller, ridge like forms (see supporting information Table S3) are shown in middle-blue and furrow or channel-like forms in pink. Dashed lines indicate inferred tributary paths (the tributary is inferred to have been buried by later deposits or removed by erosion). Small dark boxes show location of Figures 7a and 7b. Image credits NASA/JPL/UofA.

performed we identified the Transitional Unit, TMu, as a separate unit to the SMu, but HiRISE images show it to comprise a mixture of local overburden Undivided Plains and SMu type surfaces, so discussion of TMu is generally combined with SMu in the following. Exposures of the marginal units extend laterally tens to thousands of meters to either side of the Aram Dorsum main ridge and surround many of the minor ridge systems that connect with Aram Dorsum. The marginal units are consistently superposed by the continuous parts of the Aram Dorsum main ridge, but the smaller subsidiary ridges that intersect with Aram Dorsum have a more complex interleaving relationship with it (section 4.2.2). However, remnants of Aram-Dorsum-like ridges are buried within the marginal materials (Figure 5d).

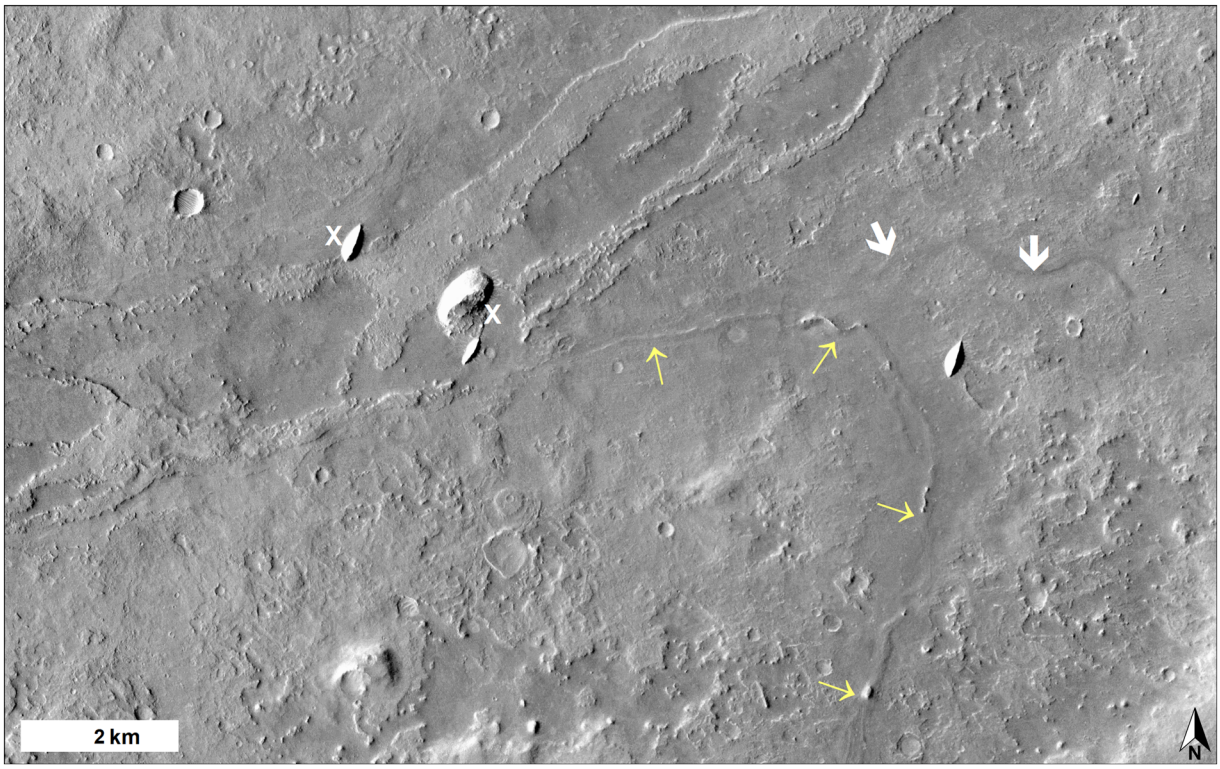

Figure 8. CTX image mosaic showing the southern branch of subsidiary Ridge 5 (fine yellow arrows) swinging to the west as it nears the Aram Dorsum main ridge. Parts of this ridge retain a resistant, flat-topped "capping unit." A faint trace of the eastern branch of subsidiary Ridge 5 can also be seen (bold white arrows), as can outliers of what are probably Etched Terrain materials (*X*) superposing the Aram Dorsum ridge. Image credit: NASA/JPL/MSSS.

The terrain comprised of the marginal units generally forms a low relief landscape, except where it contains flat-bottomed pits. At the base of these pits are surfaces containing wide fractures. The pits are up to 30 m deep with steep margins, where the SMu is eroding into small, fractured blocks visible as boulders at the base of the pit walls. Also, fresh ~100 m diameter impact craters within the SMu show blocky ejecta and there is an array of polygonal and sublinear fractures within these units (section 4.2.4). This evidence suggests that the low-relief terrains surrounding Aram Dorsum are comprised of material that is indurated enough to form steep scarps, competent enough to be subject to brittle fracturing, and block-forming when undergoing scarp retreat or impact cratering. This indicates that marginal materials are competent bedrock units, and not mantles of loose material. Finally, examples of subtle layering in the SMu can be seen where it crops out on the pit walls (Figure 9a), and there is a sparse population of 50–100 m diameter, concentrically layered circular depressions (probably ancient, heavily eroded impact craters) within the SMu (Figures 9b–9d). Both observations provide some evidence for layering with in the marginal units, but layering is not generally obvious. Thus, while meter-scale layering occurs locally, persistent layering is either not present, or is of submeter scale and cannot be easily resolved in HiRISE images.

4.2.4. The Distribution of Polygonal Fractures and Associated Small-Scale Surface Features

Decameter-scale polygonally or subpolygonally patterned ground is visible on the upper surfaces of Aram Dorsum and in units associated with it. These features can generally only be seen in HiRISE images. Certain types of polygonally patterned surfaces appear spatially associated with specific units in the study area and hence may provide information about a unit's composition, lithology, or depositional environment (e.g., if they formed subaerially). To test this hypothesis we measured their spatial distribution. We have identified five different polygonal or similar landforms types: (Figures 10a– 10c): (i) Narrow-Fracture polygons, (ii) Wide-Fracture polygons, (iii) Narrow-Ridge polygons, (iv) Vein-like ridges, and (v) "Meter-scale" polygons. We measured the distributions of these landform types by examining HiRISE images at full resolution and plotting their distributions against the study area map Figure 10d.

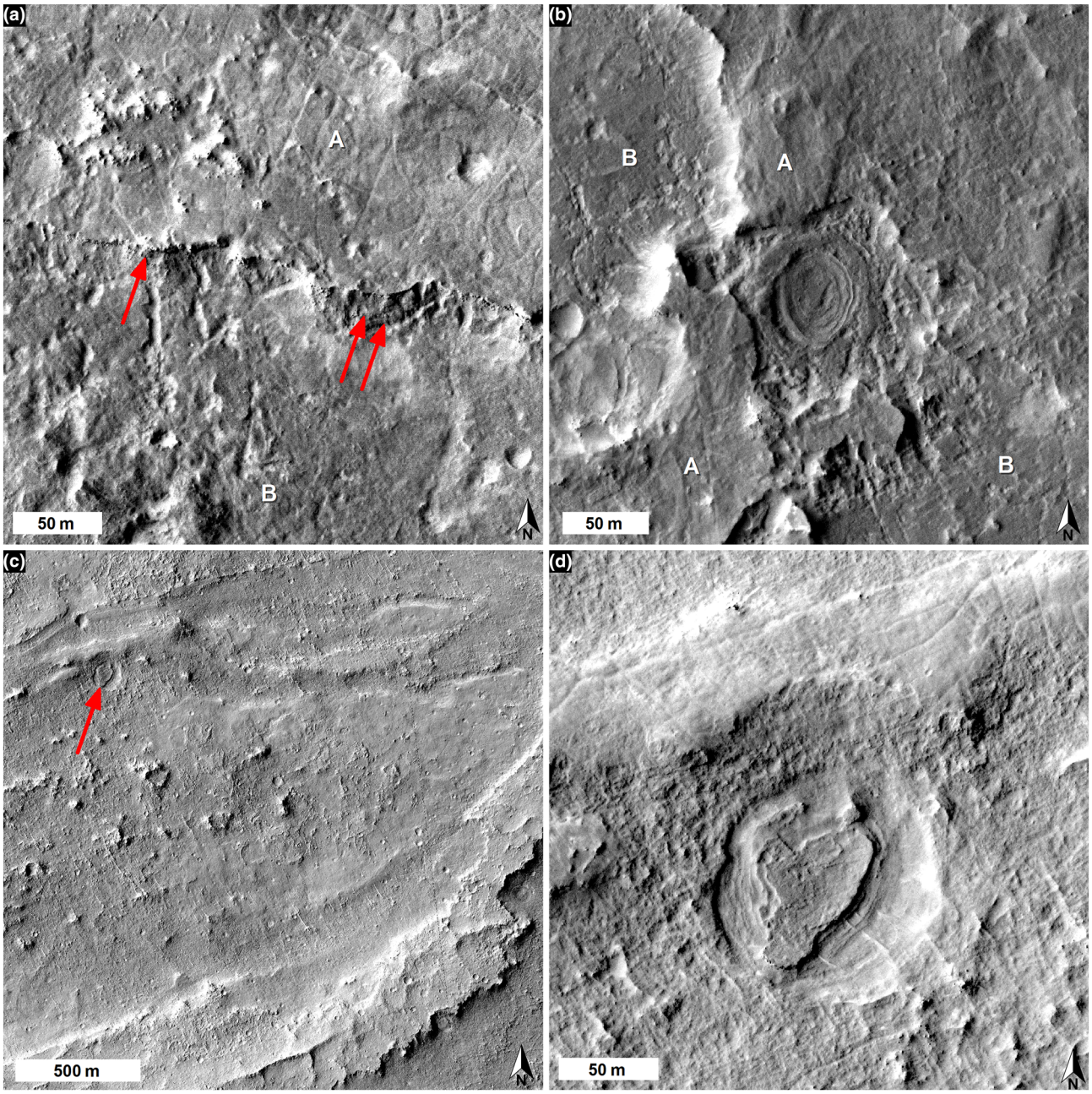

Figure 9. Examples of layering within the Smooth Marginal units. (a) Possible layering and resistant upper layer in wall of pit in Smooth Marginal material. (b) Impact crater in pit floor material (A) with Smooth Marginal material overlying it (A). The crater appears to be have been filled by layered material, which is probably from the overlying Smooth Marginal unit. (c) Approximately 100 m diameter impact crater that crosscuts the edge of a degraded branch of Aram Dorsum and adjacent Smooth Marginal unit materials. Arrow show location of (d). (d) Close-up view of small impact crater showing both that it contains a layered infill and that the crater wall itself appears to contain layers. All image credits: NASA/JPL/UoA.

Narrow-Fracture polygons occur rarely in the Aram Dorsum ridge itself, but they are common in the marginal units. Their margins are delineated by troughs or fractures <1 m across and form rectilinear to polygonal forms that are ~10–20 m across. They often superpose subsidiary ridges in the Aram Dorsum network.

Wide-Fracture polygons occur almost exclusively within flat-floored erosional pits, are ~25–50 m across, and form rectilinear to polygonal forms. Their margins are flat-bottomed troughs ~2–5 m across that penetrate through a thin layer (~1–2 m) of darker material to a higher-albedo substrate (although this brighter material could be a later infill). They often contain curved sections or discontinuous stretches with a pit-chain like

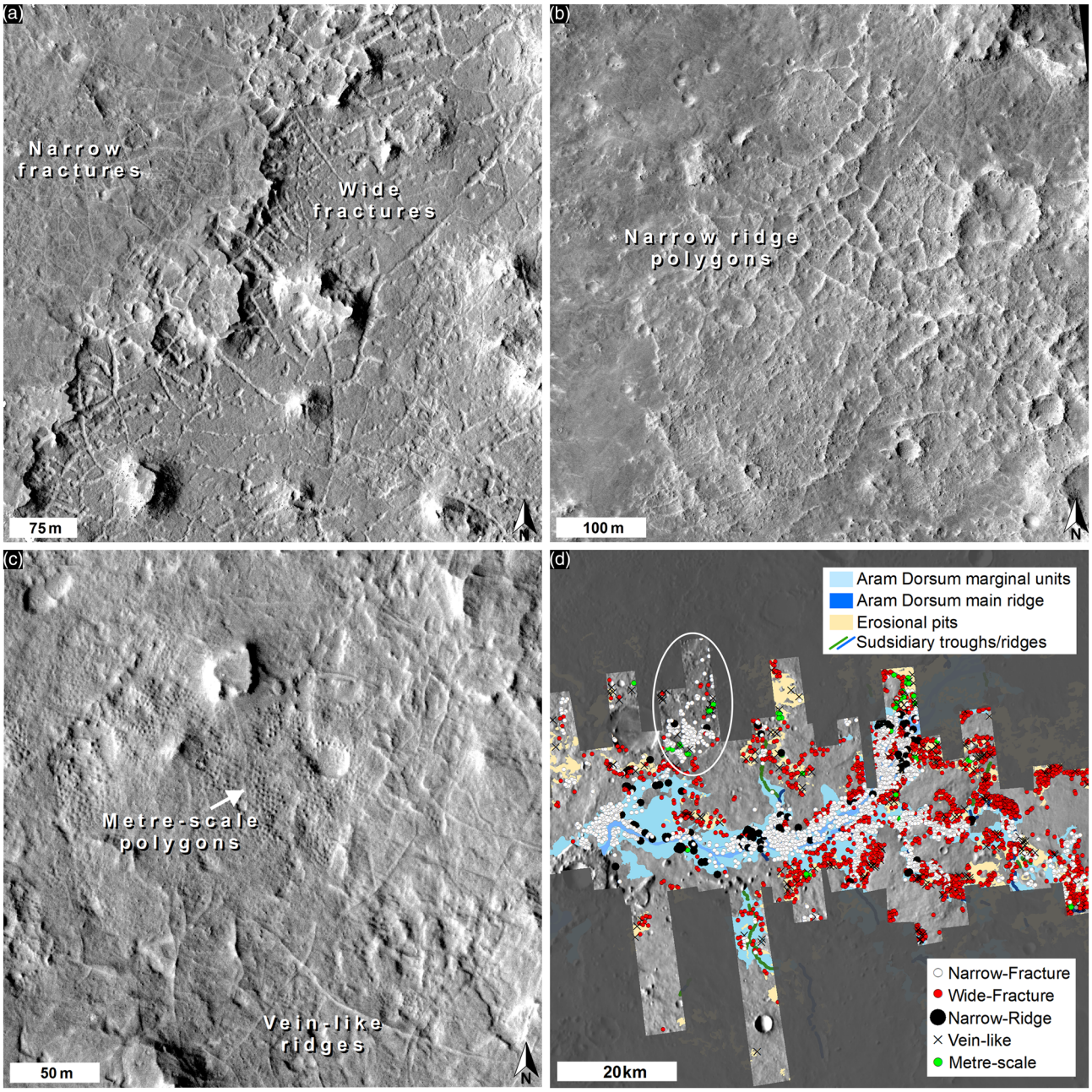

Figure 10. Examples of polygon-related landforms in the study area. (a) "Narrow-Fracture" and "Wide-Fracture" polygons. Note the discontinuous nature and pit-like form of the Wide-Fracture margin troughs. (b) Positive relief, "Narrow-Ridge" polygons. (c) "Meter-scale" polygons and "vein-like" curvilinear lineaments. (d) The spatial distribution of the different polygon types as mapped in HiRISE images. Each point represents a cluster of examples of each landform. The image is masked out (dark gray areas) where no HiRISE images were available at time of analysis. All image credits: NASA/JPL/UoA.

morphology. Where the Wide-Fracture margins become discontinuous, the network becomes more irregular until not discernable. The Wide-Fracture polygons form in surfaces subjacent to those hosting Narrow-Fracture polygons. In some examples, fractures propagate through both the lower and the overlying materials; that is, the fractures that define Wide-Fracture polygons transition directly into Narrow-Fracture polygons.

Narrow-Ridge polygons are rare compared with the previous two types, and occur in the main Aram Dorsum and marginal units. Their margins are defined by low (<1 m) ridges, not troughs, and some examples comprise closely spaced (~1 m) double pairs of ridges. They have a similar network shape and size to the

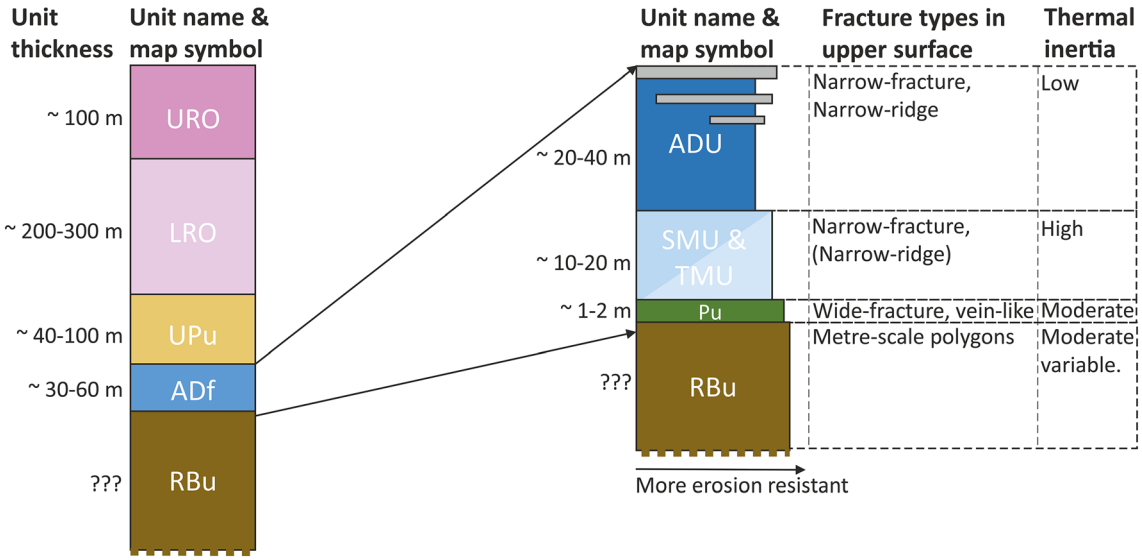

Figure 11. Schematic showing stratigraphy in the Aram Dorsum study area. ADf = Aram Dorsum formation. Unit symbols as per section 4.1. Gray elements in ADu represent resistant horizons. Vertical extent of RBu is unknown; all other vertical thicknesses derived from HiRISE DEM or MOLA measurements.

narrow-fracture ridges, which, in a few examples, they are observed to transition into. In some places, Narrow-Ridge polygons occur within a thin "veneer" of slightly rougher materials on top of surfaces containing Narrow-Fracture polygons.

Vein-like ridges occur singularly or in groups and are exclusively found in the flat-floored erosional pits and stratigraphically Rugged Basal unit. They occur as narrow ridges <1 m wide and often >100 m long, which crosscut one another to form subpolygonal patterns or clusters of subparallel lineaments. They are distinguished from Narrow-Ridge polygons by their length and upstanding, clustered outcrop pattern. They sometimes occur within and on top of Wide-Fracture polygon-bearing materials and crosscut the Wide-Fracture polygons. In rare examples they occur within the wide fractures themselves. They do not occur in materials hosting any other polygon type.

"Meter-scale polygons" occur only within basal units and flat-floored erosional pits and are rare compared to other types: Only ~50 examples of cluster of these landforms are seen out of ~4,500 observations of other polygon types. They have the form of small domes or hummocks, 1–2 m across, separated by troughs of ~1 m. Slightly larger (2–5 m) examples, with flatter tops separated by narrow fractures, occur even more rarely. This suggests that the domed examples might be remnants of a pervasively fractured planar surface. This ties in with the general setting of the Meter-scale polygons: they form beneath, or within, the degraded margins of the materials in which the Wide-Fracture polygons form.

The spatial distribution of the different types is clear: The Narrow-Fracture and Narrow-Ridge polygons are almost always associated with Aram Dorsum or its margin materials, but the Wide-Fracture, Curvilinear and Meter-scale polygons occur in the basal units or erosional pits. One area (white ellipse in Figure 10d) contains many Narrow-Fracture polygons on terrain mapped (using CTX images) as the Rugged Basal unit. However, analysis of HiRISE images show that these forms occur in small patches of smoother surfaces that could be remnant SMu material. The mapping also show a consistent stratigraphic pattern between the polygon types and the mapped units they form in the Narrow--bearing materials are youngest and superpose narrow fracture-bearing materials. These, in turn, superpose Wide-Fracture-bearing materials, which also include the Vein-Like curvilinear ridges. Finally, Meter-scale polygons appear to form beneath the materials that contain Wide-Fracture polygons and seem to be at the very bottom of the local stratigraphy (Figure 11).

4.3. Formation Age of the Aram Dorsum Ridge System and Contiguous Units

The age of Aram Dorsum is inferred by comparing the mapped units to the regional map of Greater Meridiani Planum by Hynek and Di Achille (2017), as shown in Figure 12. The unit we mapped as the

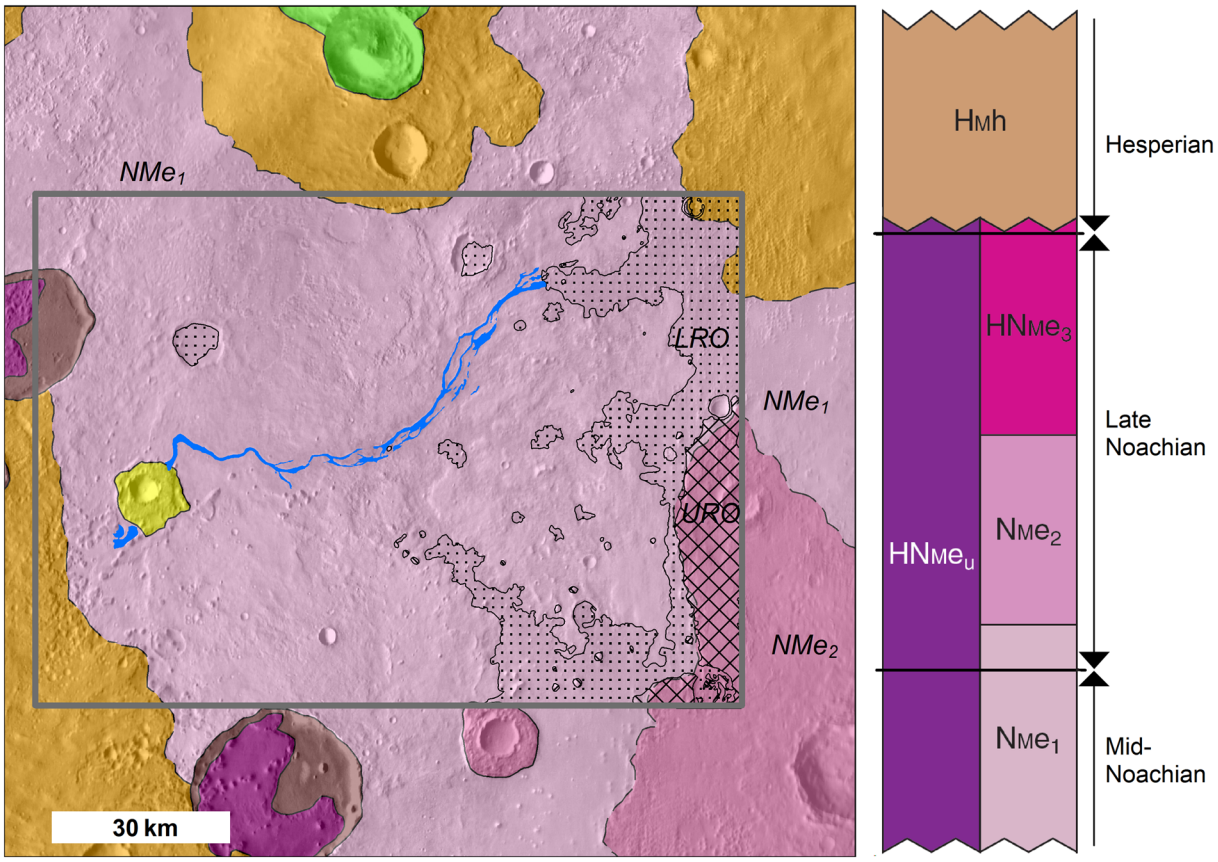

Figure 12. Selected units from this study compared with map of Hynek and DiAchille (2017). Our study area is shown by the gray box. The blue region is the Aram Dorsum unit (ADu); the dotted area is the Lower Regional Overburden unit (LRO) and the cross-hatched area the Upper Regional Overburden unit (URO). URO as mapped in this study is almost identical to the middle etched terrain unit, Nme_2, as mapped by Hynek and DiAchille (2017). A schematic representing this section of the regional stratigraphy is shown at the right, after Hynek and DiAchille (2017). This allows all units mapped in this study and superposed by our URO unit to be placed within a regional stratigraphy and given a relative age. Map credit: Hynek and DiAchille (2017) and USGS.

URO unit is equivalent to the regionally extensive NMe_2 unit of the "Etched Terrain" (Hynek & Di Achille, 2017). Our mapping at CTX-scale shows that Aram Dorsum and its marginal units are all superposed by local overburden units, which in turn are superposed by the URO and LRO units. Thus, all the terrains in our study area that are stratigraphically below the URo unit must be late-Noachian in age or older (Figure 7), as determined by Hynek and Di Achille (2017) for the NMe_2 unit.

Furthermore, it is likely that our LRO unit is equivalent to the lowest Etched Terrain unit NMe_1 of Hynek and Di Achille (2017), although there is a big differences in the areal extent of this unit between the two maps (unsurprisingly, given the very different mapping scales employed and extents covered). Our mapping was performed using 6 m per pixel CTX images, so it is likely that the generalization needed for a smaller-scale map using 100 m per pixel data means that our map is more precise and that the NMe_1 unit of Hynek and Di Achille (2017) combines units we mapped as local overburden materials with the LRO. If this is the case, then we can infer that Aram Dorsum is mid-Noachian or older, as our map shows it underlies the LRO unit.

We used impact crater size frequency data to cross compare the inference made from the stratigraphic observations and to determine formation and exposure crater retention model ages for some of the units within the study area. Five areas were studied: (i) the mapped extent of the Aram Dorsum main ridge to explore its exhumation age, (ii)–(iv) three different areas of local overburden to explore their exhumation/emplacement age (these areas extend beyond the map shown in Figure 3 but are in continuous surface types), and (v) a large region (~150 by 250 km) surrounding the Aram Dorsum study area to explore the age of the regional basement. We note that the history of burial and erosion that this area has

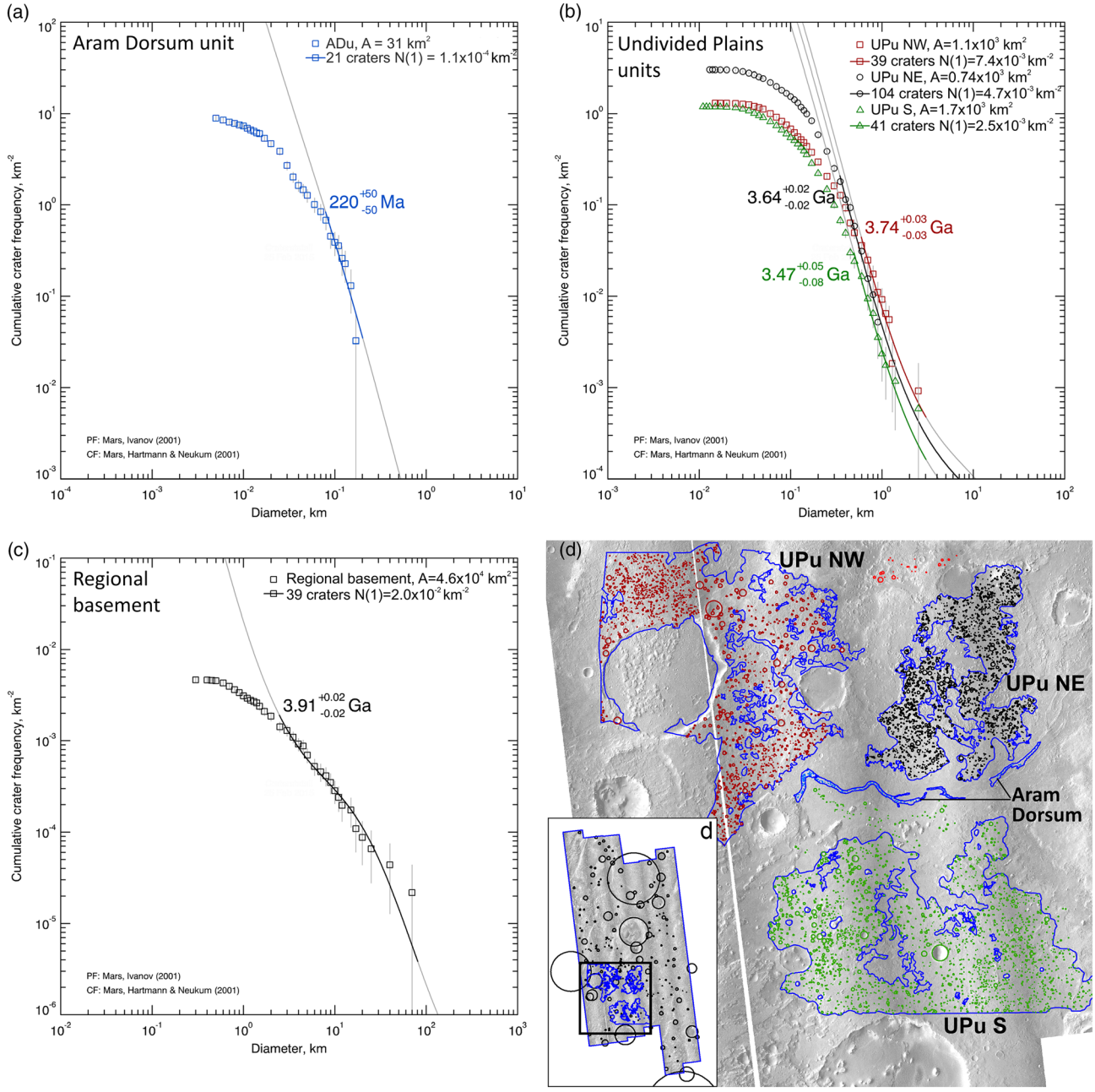

Figure 13. Crater count size frequency distribution results. (a) Aram Dorsum unit, consisting of the main flat-topped ridge (ADu). (b) Local overburden example areas from the Undivided Plains unit (UPu). See (e) for color coding by count location. (c) Regional counts of larger impact craters intended to provide a "basement" age. (d) Locations of craters counted in (c) and comparison with Aram Dorsum study area (black box). (e) Aram Dorsum study area showing the location of the crater counts shown in (a) and (b) (blue outlined areas). Individual craters are shown as colored circles that match the plots in (a) and (b): Blue = Aram Dorsum unit, red = UPu northwest, black = Upu northeast, and green = UPu south. Image is 100 km across.

experienced complicates interpretations of the results from the smaller study areas and also affects any conclusions drawn from counts of smaller diameter craters (which are more easily buried or removed). The study areas and size frequency plots are shown in Figure 9 and the results summarized in Table 1.

The crater count results show the crater retention model age for the largest craters in the region surrounding the Aram Dorsum study area is ~3.9 Ga (i.e., mid-Noachian; Michael, 2013). We interpret this as representing the crater retention age of the "basement" materials which all other units in the study area postdate. This is probably close to a formation age for the basement materials, as such large craters are not easily removed

by erosion or covered by later deposits. The Local Overburden unit crater retention model ages are younger, 3.75–3.47 Ga (i.e., late-Noachian/Hesperian; Michael, 2013), and must at least partly represent an exposure age (rather than formation age), as they have been buried and exhumed from beneath the regional Etched Terrains. Interestingly, the local overburden region furthest from the current extents of the Etched Terrain (northwest region) has the oldest age, whereas the southern region, which is still superposed by outliers of Etched Terrains, has the youngest age. Hence, it could be that the younger age represents an exposure age indicating when the overlying Etched Terrain was removed (i.e., the majority of the erosion of the Etched Terrains was during the late Noachian and into the Hesperian; in agreement with Fassett & Head, 2007), whereas the older age could be closer to the formation age of this part of the plains unit. The crater retention model age of the Aram Dorsum main ridge (~220 Ma) is representative of an exposure age, as it is unambiguously overlain by older terrains at both ends. However, the very small count area (only 30 km^2) and linear shape means this measurement is unlikely to be accurate.

Our mapping shows that Aram Dorsum was emplaced after the regional basement, but before the local overburden. This means Aram Dorsum was formed during a narrow time window between 3.91 and ~3.75 Ga, based on crater retention model ages. This agrees with the regional stratigraphic arguments that show Aram Dorsum probably formed in the mid-Noachian. Given Aram Dorsum's young (although very uncertain) crater retention model age, it has therefore either undergone significant erosion since its emplacement (to remove craters) or has been buried and protected from cratering for much of the time since it was formed. We suggest that protection from cratering was more likely, based on the superposition relationships, and that this protection was by the local and regional overburden materials. This is reinforced by the observations of outliers of older materials on top of Aram Dorsum today, showing that the areas nearest these remnants are likely to have been protected from Martian impact flux for almost all of Martian history, and are still slowly being exposed in the present day.

5. Interpretation and Discussion

5.1. Interpretation of the Aram Dorsum Ridge System

The observations that the Aram Dorsum ridge system shows (i) a large-scale ribbon-like planform, (ii) the presence of well-developed sinuous segments, (iii) the occurrence of branching sediment bodies that show patterns of connection and disconnection, (iv) the presence of ribbon form sediment bodies within the Marginal units that join the main Aram ridge from both its northern and southern margins, and (v) the presence of internal layering, all provide strong evidence that the Aram Dorsum ridge represents a “channel body” formed by a river channel system that is now preserved in inverted relief. This is similar to examples observed on Earth (e.g., Hayden et al., 2019; Maizels, 1987; Williams et al., 2011; Zaki et al., 2018). By “channel body,” we mean a sedimentary body produced by deposition during lateral and vertical accretion of depositional elements in a migrating fluvial channel over geological timescales (Friend et al., 1979). Also, Aram Dorsum is similar in many details (such as the overall ridge pattern, presence of a resistant “capping” layer and visible layering, vertical stacking, and the presence of polygonal fracturing in and around the central ridge) to other inverted fluvial channels in Arabia Terra (Davis et al., 2019, 2016) and elsewhere on Mars (e.g., Burr et al., 2010; Davis et al., 2018; Newsom et al., 2010).

Importantly, however, analysis of the Aram Dorsum ridge shows that it comprises multiple erosion-resistant ridge segments that exist at different stratigraphic levels (e.g., Figures 5d and 6a). From these observations, we infer that the Aram Dorsum ridge does not record a single fluvial channel fill deposit but rather represents several channel fill deposits that have become vertically stacked during channel belt aggradation. This leads us to interpret the linear to sinuous multi-branched ridge system that forms Aram Dorsum as an exhumed fluvial channel belt deposit that is now preserved in inverted relief, similar to Davis et al. (2019, 2016). Ridges representing inverted fluvial channel deposits on Earth also similarly comprise stacked multiple channel fills, for example, in the Caspe Formation in the Ebro basin (Martínez et al., 2010; Mohrig et al., 2000). This suggests that the Aram Dorsum ridge was formed by frequent avulsion of the active river channel, but with the channel migrating in a narrow corridor with reoccupation of former channel pathways. Channel fill stacking created multistory bodies and older, buried channels segments visible within the SMu (Figure 5d). This evidence strongly points to the Aram Dorsum ridge representing a long-lived fluvial sediment routing system rather than the deposit of a short-lived depositional event.

By analogy with terrestrial inverted fluvial systems (e.g., Hayden et al., 2019; Maizels, 1987; Williams et al., 2011), we suggest that the distinct resistant bodies are composed of indurated sandstone or conglomerate lithologies that were deposited within aggrading fluvial channels as bar deposits and channel fill sediments. Without ground-based observations of sedimentary structures and architecture it is impossible to determine the finer-scale details of the infill. Interestingly, the thermal inertia of Aram Dorsum is low relative to the adjacent marginal unit. It could be argued that a fluvial sandstone, cemented by chemicals precipitated from a solute-rich groundwater, would have a relatively high thermal inertia, as suggested for other inverted fluvial systems on Mars (Williams et al., 2018), but this signal could represent sand or dust cover trapped in a rougher surface instead.

We find no evidence that Aram Dorsum is a volcanic channel or lava-filled channel. The multilevel nature, branching-reforming channel shape, and the presence of minor resistant layers within the flanks of Aram Dorsum, all argue against this being a simple lava-filled valley. Similarly, while it could be argued this landform is an esker, there is far less evidence to support this interpretation compared to that of a fluvial channel belt: There is no other evidence of glaciation regionally; eskers generally have more sharply defined ridges, generally have lower width/height ratios, do not usually possess a continuous resistant uppermost layer, and are not observed to be set within consistent contributory networks that interfinger with marginal floodplains deposits. As pointed out by Butcher (2019), convergence of form can make distinguishing eskers and inverted channel problematic, and only by comparing geomorphic observations and mapping of the regional landscape can one hypothesis be favored over another. Here, all such evidence is consistent with Aram Dorsum being an exhumed ancient fluvial depositional complex.

A question of considerable interest (especially for inferring palaeodischarge) is whether the planform ridge width of Aram Dorsum is reflective of the width of the original active fluvial channel or is the result of lateral amalgamation of channel fill deposits both by lateral migration and jumping of the channel during avulsions. Unfortunately, the absence of preserved bedding structures on the upper surface of the Aram Dorsum ridge, like those identified in other examples of Martian palaeofluvial deposits such as in Eberswalde and Jezero craters, precludes more detailed interpretation of the planform evolution of the Aram system. Given the very broad width of the Aram ridge, however, being up to 1,200 m in breadth (which is exceptionally large for a formative channel), we suggest that Aram Dorsum was most likely formed by lateral migration or lateral avulsive translation of channels to produce a laterally amalgamated channel belt deposit as has been proposed for other ridge systems in Arabia Terra (Davis et al., 2019) and terrestrial examples in Utah (Hayden et al., 2019). The presence of multiple threads in the eastern sector of the Aram ridge is good evidence for laterally displaced channels formed by channel avulsion.

One interesting observation is the preservation of a set of large wavelength bends in the ridge planform in its western sector. Singh et al. (2017) document a similar set of bends in a channel belt deposit in the Indo-Gangetic basin but demonstrate that these are bends in an incised valley system (see their Figure 3). Thus, it is plausible that the Aram Dorsum ridge represents the exhumed deposits of fluvial channel belts that infilled a valley incised into floodplain deposits as is widely observed in the modern Indo-Gangetic basin (Singh et al., 2017). This "incised-valley fill" explanation provides one mechanism for the preservation of a sinuous ridge planform in channel belt deposits. Exhumed incised-valley fills have been inferred on Mars at Aeolis Dorsa (Cardenas et al., 2018).

In summary, we suggest that both the vertical thickness and lateral width of Aram Dorsum do not represent the dimensions of the formative river channel but rather are the time-integrated products of lateral and vertical stacking of channel fill deposits to form multistory and multilateral sedimentary bodies (Friend et al., 1979). Such an interpretation is consistent with terrestrial examples, but without in situ analyses of outcrop level information, more robust inference is impossible.

We interpret the narrow subsidiary ridge systems as the preserved remnants of smaller fluvial palaeochannel bodies that form part of the overall Aram Dorsum fluvial routing system. The observations that they occur on either side of the main Aram Dorsum ridge, have similar morphology, that none of the subsidiary ridges slope away from Aram Dorsum, and that the subsidiary ridges approach or join the main Aram Dorsum ridge all provide strong evidence that the two types of ridge systems are genetically related. We conclude that the subsidiary ridge systems formed a tributary fluvial drainage network that fed into the main Aram Dorsum river. In some examples (e.g., Figure 7b), the tributary ridges show complex forms, or lie atop of

flat, platform-like ridges, consistent with the presence of multiple resistant horizons within the ridge, and hence perhaps evidence for channel stacking. However, their small scale and significant degree of erosion makes it harder to interpret this evidence here than in the main Aram Dorsum ridge.

The acute junction angles where the subsidiary ridge systems join or approach Aram Dorsum, with closure to the west, suggest flow in Aram Dorsum was east to west (cf., Hackney & Carling, 2011). Furthermore, although postdepositional modification makes it hard to identify their source regions, the various subsidiary palaeochannels appear to originate from points with a range of elevations and from a spatially distributed region. Where best preserved, these tributaries have relatively high stream orders (up to 3 or 4) and have low gradients over tens of kilometers. Only a few of these ridges have retained a resistant capping layer, consistent with these being smaller fluvial systems whose resistant elements were more easily removed by erosion compared to the main Aram Dorsum ridge.

For terrestrial rivers, one measure of the spatial dissection is drainage density, the ratio of total river length to drainage area. For Aram Dorsum, a comparable metric can be crudely estimated based on the modern exposure of the ridge complex. The total length of exposed channel in the study area, determined from the mapped tributary ridge network (Figure 7c), is ~360 km. The drainage area estimate, found by connecting the upslope endpoints of first order ridge segments, is ~3,800 km^2, giving a drainage density of ~0.1 km^{-1}. It is likely that the drainage area is an underestimate, because (i) channel heads are rarely located at drainage divides and (ii) lower order streams may not have been preserved. Also, as this method assumes simultaneous flow throughout the system, it may overestimate the total path length, but we suggest that this effect is roughly offset by incomplete preservation of the flow pathways. Given these uncertainties, we suggest that a drainage density estimate of 0.1 ± 0.05 km^{-1} seems reasonable. We note that this is comparable to the highest values measured for Martian valley networks (up to 0.2 km^{-1}; Hynek Beach & Hoke, 2010).

Although there are no distinct features that enable an unambiguous interpretation of the smooth Aram Dorsum marginal unit, the interpretation of the main Aram Dorsum ridge as a fluvial channel belt deposit with smaller contributory palaeochannels joining it strongly suggests that the marginal materials represent overbank sedimentary deposits that accumulated in a floodplain belt on either side of the main Aram Dorsum ridge (e.g., Pizzuto, 1987). These deposits probably comprise mudstones and fine sandstones deposited in a low energy environment due to bank overspill from adjacent fluvial channels during flood episodes. However, given that the caprock resistant beds that comprise the top of Aram Dorsum and many of its contributory minor channels generally lie several meters to tens of meters above the SMu surfaces, these surfaces cannot represent the last active floodplains. Instead, if they are overbank deposits, then they have been exhumed from beneath at least a few tens of meters of similar material. The lateral continuity of the unit and its relatively uniform character over large parts of the terrain add support to an overbank/floodplain alluvial environment. The presence of subtle internal layering, as indicated by the occurrence of interstratified more resistant lithologies, which form scarps and cliff-like edges at the margins of pits, suggests variation in lithological succession in these materials. We also observe that the Aram Dorsum segments buried by the smooth marginal material (Figure 5) are indicative of fluvial channel ridges being exhumed from within a more extensive overbank deposit cover. Small, degraded impact craters, sometimes with layered infill (Figure 9), within the SMu also indicate a sedimentary nature for the units and possible hiatuses during long-term accumulation of the overbank unit.

5.2. Implications of Polygonal Fracturing and Related Landforms

It is almost impossible to ascertain the origin of the polygonal and subpolygonal forms observed here, but some key interpretations can be drawn: (i) the Narrow-Ridge polygons appear to represent erosion-resistant fills of fractures similar in form and scale to the Narrow-Fracture polygons; (ii) the continuity of fractures between Narrow and Wide-Fracture polygons, and the observation of fracturing on the subsidiary ridges, shows they penetrate deeply and across unit boundaries; (iii) the Vein-like ridges appear to represent erosion-resistant fills in longer, less organized fractures than the Narrow-Ridge polygons, and at a lower stratigraphic level; and (iv) because the landforms described here are associated with specific units and surface types, they can help us understand the stratigraphy of the Aram Dorsum-related materials and demonstrate that this stratigraphy is consistent across the study area. A first order interpretation of this stratigraphy is shown in Figure 11.

The Narrow-Fracture and Narrow-Ridge polygons, seen in the Aram Dorsum inverted channel and the SMus, are superficially similar in form to Martian fractures thought to have formed by thermal contraction in ice-rich sediment, or by desiccation (e.g., El Maarry et al., 2010; Levy et al., 2009). If they formed this way, they would represent a palaeosurface. However, as they persist across unit boundaries, crosscut small inverted fluvial ridges and are visible in the SMu material, despite it having undergone tens of meters of erosion, this interpretation seems unlikely. The fractures instead are likely to have formed after deposition and lithification of the sediments, probably due to burial and/or reexposure unloading or hydrofracture. This is a reasonable interpretation: The whole Aram Dorsum study area was buried by regional Etched Terrains (remnants of which are hundreds of meters thick) or local overburden units, and much of the terrains visible here has clearly been exposed by erosion. The Narrow-Ridge polygons are probably inverted forms of the Narrow-Fracture polygons, which somehow became more resistant than their surrounding channel body materials—perhaps by deposition of minerals by groundwater flow or by infill of more resistant debris.

The Wide-Fracture polygons form in materials that are consistently beneath the other Aram Dorsum group units. They may represent similar fracture types to the Narrow-Ridge polygons, but have a different form because they occur in a material of different lithology or thickness. The "Meter-scale polygons" are difficult to interpret. They appear to be either a degraded form of the material in which the Wide-Fracture polygons form in, or are a feature of the underlying basal materials. Nevertheless, they always occupy a consistent position in the local stratigraphy, below materials containing other types of polygon-like forms.

The Vein-like curvilinear ridges are always found stratigraphically and topographically below the main Aram Dorsum inverted channel and marginal deposits. They have a morphology suggestive of mineralized veins or fracture fills. This would be consistent with a subsurface formation by mineralized groundwater exploiting fractures or voids and depositing resistant minerals, later exposed by erosion as curvilinear forms. Their low-angle crosscutting patterns suggest that several generations of fracturing (rather than fracture re-activation) and mineral deposition occurred. Groundwater deposition is a plausible hypothesis given the fluvial interpretation of the units that lie stratigraphically above and spatially close to these lineaments, and similar interpretations have been made for such features elsewhere on Mars. For example, in Gale Crater, Mg-rich diagenetic ridges (Bridges et al., 2015; Léveillé et al., 2014), late diagenetic sulfate veins (Schwenzer et al., 2016), and other mineralized fracture fills of centimeter to decameter scale (e.g., Kronyak et al., 2019; Siebach & Grotzinger, 2014) are present at various points in the ancient fluviolacustrine succession.

The Narrow-Fracture/Narrow-Ridge polygons in particular are widespread and appear to be "marker landforms" for smooth marginal materials interpreted to be overbank deposits or for the inverted channel deposits themselves. Future work to analyses the size distribution and network shape of the polygonal fractures, and more measurements of the thicknesses of the units in which they occur, could help determine their origin. HiRISE image-based comparisons of Aram Dorsum with the many other inverted fluvial channels systems could reveal if these spatial and stratigraphic relationships reoccur in fluvial inverted channels regionally or globally; they certainly occur in several other inverted channel systems on Mars (Davis et al., 2019; Newsom et al., 2010).

5.3. What Time-Scale Does the Aram Dorsum Palaeo-Fluvial System Represent?

The observation that the Aram Dorsum ridge forms a depositional complex consisting of laterally and vertically stacked channel bodies suggests that the Aram fluvial system was formed by long lived fluvial activity over a geologically long time span. Timescales of fluvial channel belt longevity are poorly constrained on Earth, partly because fluvial stratigraphy preserves time highly incompletely and sediment accumulation rates are highly variable. Fluvial deposition was likely intermittent and the depositional record within the inverted channel belt deposit almost certainly represents a small fraction of the overall time that fluvial systems were active. For example, Singh et al. (2017) show an ~25 m thick stack of fluvial channel deposits in which younger fluvial deposits are inset into similar fluvial deposits, across an erosional surface, that are ~40 kyr older, demonstrating significant time gaps between deposition.

The exposed alluvial sequence comprises at least 15–40 m thickness of Aram Dorsum ridge material (fluvial sandstones and interbedded overbank deposits), 10–20 m thickness of SMu material (overbank deposits), and, beneath these units, a few meters of materials containing Wide-Fracture polygons (of unknown

origin, but appearing to be related to the Aram Dorsum overbank deposits). The exposed alluvial deposits at Aram Dorsum therefore have 30–60 m of vertical thickness. The surface area of the Aram Dorsum formation surface exposed in the study area is ~1,200 km^2. This equates to an original volume of sediment of about 4–6 km^3 within the study area.

A meta-study (Colombera et al., 2015) comparison of terrestrial studies of fluvial aggradation rates in fluvial sequences of similar channel belt widths to Aram Dorsum found aggradation rates of 0.01–0.7 m/kyr (most studies being in the 0.02–0.2 m/kyr range) measured over 10^5–10^7 year timescales. Applying these rates to the thickness of alluvial sedimentary material exposed at Aram Dorsum gives a deposition duration of 0.04–6 Myr. Although these terrestrial studies are clearly not a direct comparison for Mars, and at present the specific depositional environment is not well known, we suggest that 10^5–10^7 years is a plausible estimate for the time taken to deposit the Aram Dorsum system. This is similar to the inferred minimum timescales of formation of the valley networks (Hoke et al., 2011) and is longer than predicted durations of individual transient warming events triggered by impacts or volcanism (Halevy & Head, 2014; Segura et al., 2002; Toon et al., 2010). However, as noted above, fluvial sedimentary deposits are often incomplete in their preservation of time (e.g., Durkin et al., 2018; Sadler, 1981), and sediment accumulation rates can be highly variable (e.g., Badgley & Tauxe, 1990; McRae, 1990), so the depositional record seen at Aram Dorsum probably represents a fraction of the overall time that the fluvial system was active.

5.4. Source of Water

The main trunk of Aram Dorsum can only be seen for <100 km of its length, as it is buried by younger deposits at each end. It almost certainly connected with other similarly large inverted channels in the Arabia Terra region (Davis et al., 2016), forming what was once a regionally connected river network, but no definitive observations have yet been made to prove this link. It is clear that the source of some, or perhaps most, of the water that flowed through the Aram Dorsum river system was from outside of the study area, and its origin cannot be determined. However, the Aram Dorsum river was not simply a conduit for water and sediment; many subsidiary channels fed into the main river, and these have their sources at various locations and heights within the study area. This is consistent with a locally distributed origin for the water, such as precipitation of rain or melting of snow. The network of subsidiary channels is inconsistent with a single, or even relatively distributed, source of water from far outside the study area (e.g., from melting icecaps in the southern highlands; Fastook & Head, 2015; Wordsworth et al., 2015). Hence, the morphology of the Arabia Terra inverted channel belt system demonstrated both a regional influx of water from elsewhere in western Arabia Terra, and a distributed, local source of liquid water.

5.5. When Was Aram Dorsum Deposited?

The mapping and impact crater size frequency analysis performed here demonstrates that the Aram Dorsum river system almost certainly formed during the mid-Noachian. This is before the peak of valley network-forming fluvial activity in the southern highlands, thought to have been in the late-Noachian to early Hesperian (e.g., Fassett & Head, 2008b; Howard et al., 2005; Irwin, Howard, et al., 2005). We note that the aggradational fluvial activity at Aram Dorsum and elsewhere in Arabia Terra (Davis et al., 2016) also contrasts with the mainly erosional fluvial style associated with later valley network formation.

Fluvial activity at Aram Dorsum also therefore occurred before the formation of the Hesperian volcanic plains (Carr & Head, 2010), considered as a possible source of short-lived, episodic climate-changing volcanism (Halevy & Head, 2014). However, the mid-Noachian age does coincide with the beginning of the formation of the Tharsis volcanic rise (Carr & Head, 2010; Fassett & Head, 2011; Phillips et al., 2001). The formation of Tharsis caused substantial loading and deformation of the elastic lithosphere (e.g., Phillips et al., 2001), as well as migration of the location of the rotational pole of Mars (e.g., Citron et al., 2018; Perron et al., 2007) and recent work suggests that Tharsis formation could have caused as much as 1 km of downward vertical deformation at the Aram Dorsum study area (Citron et al., 2018; supporting information Figure S2). The same study suggests that an early-mid-Noachian Martian ocean was present prior to the formation of most of the volume of Tharsis (Citron et al., 2018) and that it had a shoreline close to the elevation of Aram Dorsum (Carr & Head, 2003; Clifford & Parker, 2001). Hence, the formation of Aram Dorsum could have been influenced both by the presence of a shoreline, and by significant changes in base level if it debouched into an ocean. We note that

similar conclusions, albeit for a later early-Hesperian ocean/large lake system, were drawn by Cardenas et al. (2018) in a study of fluvial systems in the Aeolis region. This suggests integrated fluvial systems, controlled by base level variations in large standing bodies of water were present during both the mid-Noachian and early Hesperian periods.

5.6. Implications for the Noachian Martian Environment

Aram Dorsum was emplaced as an aggradational fluvial system over 10^5–10^7 years during the mid-late Noachian. It was a major river network that formed just one of many similar water sediment routing systems in Arabia Terra. To allow the construction of the observed channel architecture, flow must have been relatively sustained over geological time period, rather than catastrophic, so liquid water must have been stable here for substantial time periods. The observation of high drainage densities and distributed local sources of water around Aram Dorsum, as well as the regional network of ancient aggradational river systems (Davis et al., 2019, 2016), shows that precipitation of rain or melt of snow must have occurred, and that flow was relatively persistent. We suggest that this scenario is consistent with a climate that supports long-lived warm and wet (relative to present-day Mars) equatorial environments and regional precipitation (e.g., Craddock & Howard, 2002; Di Achille & Hynek, 2010; Hoke & Hynek, 2009; Irwin, Howard, et al., 2005; Ramirez & Craddock, 2018), rather than a cold and dry global climate, punctuated by short-lived periods of melting, and highly localized sources of water in the southern highlands (e.g., Fastook & Head, 2015; Wordsworth et al., 2013, 2015). Furthermore, the elevation of Aram Dorsum (~−2,000 m) is far below the predicted ice stability elevation of ~1,000 m predicted in Late Noachian Icy Highland models (Fastook & Head, 2015; Wordsworth et al., 2013), in disagreement with a local source of water from melting icecaps in the Aram Dorsum study area. The observation of vein-like forms low in the local stratigraphy, and polygonal ridges within the SMus suggest the deposition of resistant minerals from groundwater in this area. The timing of this groundwater activity is impossible to determine, but it must have been after the fluvial sediments in the region became indurated, to allow flow within fractures.

The timing and likely duration of activity at Aram Dorsum argues against the source of water being precipitation during warm climate excursions caused by intense volcanism or 100 km- scale impact crater formation, both of which are thought to have short durations (~10^1–10^2 years) climatic effects (e.g., Halevy & Head, 2014; Palumbo & Head, 2018; Segura et al., 2002; Toon et al., 2010). It is possible that the cumulative effects of many such events could have generated a sufficiently long 'precipitation-supporting period' for Aram Dorsum to form, but this would have required hundreds of millions of years for such a period to accrue (Palumbo & Head, 2018), which does not agree with the geological history interpreted from our mapping.

Possible base level changes associated with the growth and retreat of an ocean in the northern plains, coupled with the formation of Tharsis and its attendant effects on lithospheric deflection and the position of Mars' rotational pole, could also have been important in how Aram Dorsum evolved, if such events occurred. We speculate that the formation of multiple aggradational fluvial systems in Arabia Terra may have been driven by such global-scale processes, alongside a long-lived relatively "warm and wet" climate. Testing whether fluvial activity at Aram Dorsum was governed by global-scale changes in the Martian environment requires further analysis and will probably need a synthesis of the geological history and stratigraphic setting of many other fluvial features in this area. This is a challenging proposition, as it requires many systems to be investigated at the highest resolution, correlative morphostratigraphic mapping performed at comparable scale (i.e., using 6 m per pixel CTX data), and detailed morphological observations made using HiRISE images of multiple systems.

5.7. Proposed Landscape Evolution Model

Figure 14 illustrates how we interpret the Aram Dorsum system to have developed. The oldest terrains in the study region probably reflect topography created by large craters and their ejecta during the earlier parts of the Noachian (Figure 14a), which underwent significant amounts (and possibly multiple episodes) of erosion, burial, and exhumation. During the mid-Noachian, precipitation within the study region, and influx of water and sediment from outside it, created a river system that initially flowed within a landscape reflecting the preexisting impact-created relief. As the river system developed, it formed bank-stabilized channels set in flat-lying floodplains (Figure 14b). Further sedimentation altered the topography, causing the

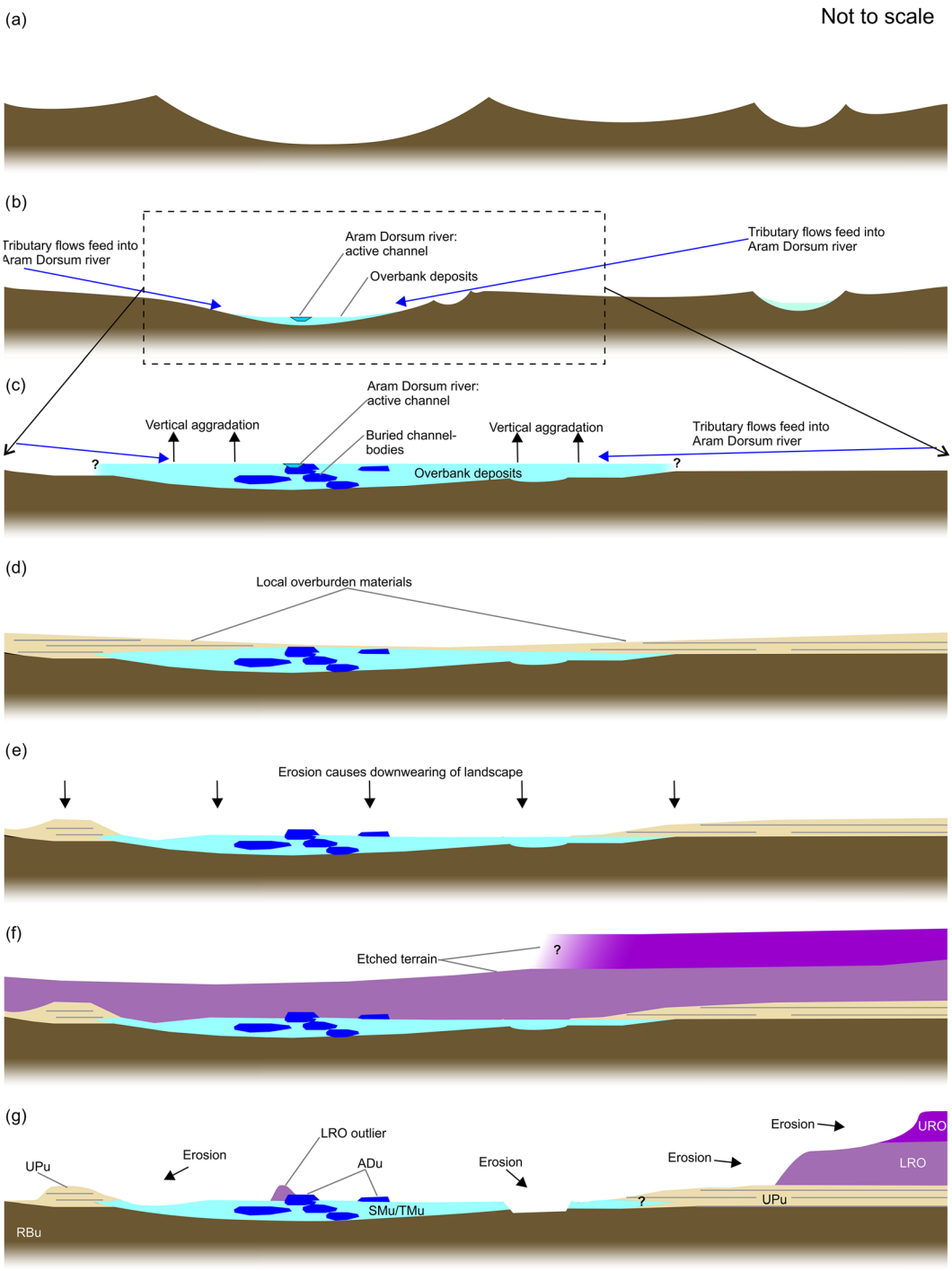

Figure 14. Interpreted evolution of Aram Dorsum and surrounding area. (a) The earliest Noachian terrains in the region represent relief created by the action of impact craters, volcanism, and other minor processes. (b) The early Aram Dorsum river system flowed through the preexisting impact-created relief, eventually forming bank-stabilized channels within flat-lying floodplains. It is likely that smaller tributary systems also flowed into the main Aram Dorsum river and that other areas of low-elevation in western Arabia Terra also hosted similar fluvial systems. Impact cratering and erosion continued to shape the surface. (c) Further sedimentation caused channel(s) to both avulse laterally and aggrade vertically, building multistory fluvial sand bodies set within thicker deposits of finer-grained floodplains and overbank deposits. (d) After Aram Dorsum became inactive, it was buried by "local" overburden materials of variable thickness. These materials are interpreted to be impact crater ejecta from the local (~100 km) region. (e) Following burial by local overburden, Aram Dorsum was reexposed by erosion and then (f) reburied by regionally extensive "etched terrain" materials. (g) Finally, relatively low intensity erosion occurred throughout the Hesperian and Amazonian periods, removing significant amounts of materials but left outliers of etched terrains exposed. The erosion-resistant channel bodies in Aram Dorsum were exposed in inverted relief because the more erosion-susceptible overbank deposits were preferentially removed. The last panel of the diagram includes map unit labels, to illustrate how the evolution of the area was inferred from the mapping.

channels to both avulse laterally and aggrade vertically. This built multistory fluvial sand bodies set within thick deposits of finer-grained floodplains and overbank deposits (Figure 14c). These fluvial sediments were at least 40–60 m thick, based on current exposure.

After the Aram Dorsum river systems became inactive, the study area underwent multiple periods of burial and erosion during the mid-late-Noachian and early Hesperian (Figures 14d and 14e). Initial burial of up to tens or hundreds of meters thickness was probably by impact ejecta but other sources including volcaniclastic, eolian, and perhaps even late stage fluvial deposition cannot be ruled out. The last major burial event (Figure 14f), of at least 300 m thickness in the central to eastern part (possibly wider) portion of the study area, was by the regional Etched Terrains (e.g., Hynek & Di Achille, 2017; Hynek & Phillips, 2008), and outliers of this terrain type can still be seen across the study area. Total burial depth in this region was estimated to be up to several hundred meters by Zabrusky et al. (2012).

As they became inactive and were buried, the Aram Dorsum channel and overbank sediments were lithified, probably due to the formation of chemical cements (Williams et al., 2018) or by compaction caused by the emplacement of overburden materials. Those fluvial sediments deposited within active channels became coarse-grained channel body sandstone and conglomerate lithofacies, and those sediments deposited in the floodplains or during overbank events became mudstones and finer-grade sandstone overbank lithofacies. The fluvial sediments within the Aram Dorsum valley area were probably also a groundwater routing pathway, as shown by the presence of what we interpret to be mineralized veins in the lower parts of the Aram Dorsum local stratigraphy. It is possible that the presence of continuous ribbon-like bodies of coarse grained sand could have provided optimal, permeable groundwater transport conduits (as on Earth; e.g., Fogg, 1986; Miall, 1988) that were of regional importance. However, the specific details of how and when groundwater flow occurred here are hard to constrain.

Our mapping suggest that there must have been some erosion of the local overburden materials mapped as the Undivided Plains units prior to burial by the Etched Terrains (which unconformably overlie all the older units in the region). This could be due to relatively shallow burial if the undivided plains are composed mainly of impact ejecta: there are several 30–50 km diameter impact craters that appear to postdate Aram Dorsum and lie within 50–75 km of it. These craters are each approximately two crater radius distances away from Aram which, given that ejecta mobility (rim-to-ejecta distance divided by crater radius) in the Martian equatorial region is generally 1.2–1.8 (Robbins & Hynek, 2012), could explain both why this material was easily removed, and why Aram Dorsum now appears to occupy a regional topographic low, surrounded by thicker ejecta material. It is possible, therefore, that some or all of the Aram Dorsum alluvial facies were exposed prior to emplacement of the Etched Terrains. Noachian erosion rates of ~1 m/Myr (Golombek et al., 2014) are consistent with the thinner parts of the local overburden being removed, but unpicking the detailed history of burial and erosion here will probably require more detailed mapping using HiRISE images and DEMs.

Following burial by hundreds of metrs of local overburden materials and Etched Terrains, subsequent erosion then removed much of this protective covering from the study area, until the part of the Aram Dorsum alluvial system seen today was exposed (Figure 14g). Estimates of Hesperian and Amazonian erosion rates of <0.01 m/Myr (Golombek et al., 2014) suggest <50 m of post-Noachian downwearing, but the Etched Terrain at least appears more susceptible to erosion than typical Martian terrain (Hynek et al., 2002), so removal of hundreds of metrs of thickness appears plausible. Once Aram Dorsum was exhumed from beneath overburden materials, the erosion-resistant, cemented channel body sandstone/conglomerate lithofacies underwent slower downwearing than the surrounding, finer-grained overbank deposits, leaving the Aram Dorsum channel bodies upstanding as ridges. This created the landscape observed today.

6. Conclusions

Our observations and mapping reveal Aram Dorsum to be the sedimentary deposits of an extensive aggradational fluvial channel belt system that was could have been active for durations of 10^5–10^7 years. Both stratigraphy and crater counting suggest that this river system was active in the mid- to late-Noachian, before the period of peak activity of the Valley Networks. The section of Aram Dorsum currently visible is up to about a kilometer wide and nearly 100 km long. Aram Dorsum was therefore a sizable, ancient, long-lived fluvial system.

The Aram Dorsum formation comprises a succession of what are, by analogy with terrestrial fluvial systems, probably coarse-grained fluvial channel belt sandstones and finer-grained overbank deposits. At least 40–60 m vertical thickness (equivalent to several cubic kilometers) of fluvial sediments are found here. Other inverted channels elsewhere in Arabia Terra (e.g., Davis et al., 2016; Newsom et al., 2010) have similar characteristics (e.g., length, width, planview morphology, polygonal fractures, and ridges), suggesting that similar thicknesses and volumes of mid-Noachian to late-Noachian fluvial sediments may be extensive and common in this region. Selective regional preservation and exposure also mean that more fluvial sedimentary rocks are probably buried beneath the regional Etched Terrains, so the true extent of the fluvial succession in Arabia Terra could be even greater.

The various polygonal fractures seen in the Aram Dorsum study area probably reflect brittle failure as a result of burial and/or unloading, while vein-like ridges probably reflect deposition and alteration of materials by groundwater in underground fracture networks. There is a consistent stratigraphic and spatial relationship between these landforms, which suggest they are genetically related to specific sedimentary facies within the Aram Dorsum formation. Future studies of other inverted channels in this region could test this hypothesis.

Observations of a series of smaller river systems feeding Aram Dorsum, sourced from various palaeoelevations and locations in the study area, suggest a distributed source of water. The Aram Dorsum main channel belt was also supplied with water from upstream of the study area, with flow from east to west, and its scale is consistent with a large catchment. Together, this evidence suggests that local and regional precipitation (either as rain or as seasonal or repeated snow melt) was the source of water. Furthermore, observations of similarly ancient large inverted channels systems in Arabia Terra (Davis et al., 2019, 2016) provide evidence that precipitation was widespread across western Arabia Terra during this period.

Evidence for precipitation, possible groundwater deposition of mineralized veins, and Aram Dorsum's low elevation and distance from the majority of the Valley Networks, argues against the source of water being melting of a distant, high-altitude, ice sheet, or ice cap. Similarly, the aggradational fluvial depositional setting and the scale of the system do not suggest deposition from multiple short-lived fluvial flows, as might have occurred due to impact cratering or catastrophic volcanic outgassing temporarily altering the climate.

We conclude that Aram Dorsum presents a sedimentary record of mid-Noachian fluvial processes, and that the system was laid down in a climate conducive to precipitation and stable flow of liquid water.

Acknowledgments

M. R. B. acknowledges UK Space Agency funding (ST/L00643X/1 and ST/R001413/1), S. G. acknowledges UK Space Agency funding (ST/L006413/1 and ST/S001492/1), J. M. D. acknowledges STFC and UK Space Agency funding (ST/K502388/1 and ST/R002355/1), P. F. acknowledges UK Space Agency funding (ST/R001413/1), P. M. G. acknowledges UK Space Agency funding (ST/L00254X/1). R. M. W. acknowledges NASA "Odyssey Participating Scientist" and NASA MDAP 80NSSC19K1216 funding. A list of CTX and HiRISE images used is given in Table S1 in the supporting information to this paper. CTX and HiRISE image data are publically available at the NASA Planetary Data System repository in the Mars Reconnaissance Orbiter section (https://pds-imaging.jpl.nasa.gov/portal/mro_mission.html). The mapping data shown in Figures 3 and 10 and the map description in the supporting information are publically available online (at https://ordo.open.ac.uk/authors/Matt_Balme/8445438).

References

Andrews-Hanna, J. C., Zuber, M. T., Arvidson, R. E., & Wiseman, S. M. (2010). Early Mars hydrology: Meridiani playa deposits and the sedimentary record of Arabia Terra. *Journal of Geophysical Research Planets*, *115*, E06002. https://doi.org/10.1029/2009JE003485

Arvidson, R. E. (2005). Spectral reflectance and morphologic correlations in Eastern Terra Meridiani, Mars. *Science*, *307*, 1591–1594. https://doi.org/10.1126/science.1109509

Badgley, C., & Tauxe, L. (1990). Paleomagnetic stratigraphy and time in sediments: Studies in alluvial Siwalik Rocks of Pakistan. *J. Geol.*, *98*, 457–477. https://doi.org/10.1086/629419

Balme, M. R., Berman, D. C., Bourke, M. C., & Zimbelman, J. R. (2008). Transverse Aeolian Ridges (TARs) on Mars. *Geomorphology*, *101*, 703–720. https://doi.org/10.1016/j.geomorph.2008.03.011

Bibring, J.-P. (2006). Global mineralogical and aqueous Mars history derived from OMEGA/Mars Express data. *Science*, *312*, 400–404. https://doi.org/10.1126/science.1122659

Bibring, J.-P., Soufflot, A., Berthé, M., Langevin, Y., Gondet, B., Drossart, P., et al. (2004). OMEGA: Observatoire pour la Minéralogie, l'Eau, les Glaces et l'Activité. In A. Wilson (Ed.), *Mars Express: the scientific payload. Scientific coordination: Agustin Chicarro. ESA SP-1240* (pp. 37–49). Noordwijk, Netherlands: ESA Publications Division.

Bridges, J. C., Schwenzer, S. P., Leveille, R., Westall, F., Wiens, R. C., Mangold, N., et al. (2015). Diagenesis and clay mineral formation at Gale Crater, Mars: Gale Crater Diagenesis. *Journal of Geophysical Research Planets*, *120*, 1–19. https://doi.org/10.1002/2014JE004757

Burr, D. M., Williams, R. M. E., Wendell, K. D., Chojnacki, M., & Emery, J. P. (2010). Inverted fluvial features in the Aeolis/Zephyria Plana region, Mars: Formation mechanism and initial paleodischarge estimates. *Journal of Geophysical Research Planets*, *115*(E7), E07011. https://doi.org/10.1029/2009JE003496

Butcher, F. E. G. (2019). *Wet-based glaciation on Mars (phd)*. The Open University.

Cardenas, B. T., Mohrig, D., & Goudge, T. A. (2018). Fluvial stratigraphy of valley fills at Aeolis Dorsa, Mars: Evidence for base-level fluctuations controlled by a downstream water body. *GSA Bulletin*. https://doi.org/10.1130/B31567.1

Carr, M. H. (1987). Water on Mars. *Nature*, *326*, 30–35.

Carr, M. H., & Head, J. W. (2003). Oceans on Mars: An assessment of the observational evidence and possible fate. *J Geophy Res*, *108*(E5), 5042. https://doi.org/10.1029/2002JE001963

Carr, M. H., & Head, J. W. (2010). Geologic history of Mars. Mars Express 6 Years Orbit Mars Geol. Three-Dimens. Mapp. High Resolut. *Stereo Camera HRSC Exp.*, *294*, 185–203. https://doi.org/10.1016/j.epsl.2009.06.042

Christensen, P. R., Bandfield, J. L., Hamilton, V. E., Ruff, S. W., Kieffer, H. H., Titus, T. N., et al. (2001). Mars Global Surveyor thermal emission spectrometer experiment: investigation description and surface science results. *J Geophys Res*, *106*, 23,823–23,872.

Citron, R. I., Manga, M., & Hemingway, D. J. (2018). Timing of oceans on Mars from shoreline deformation. *Nature*, *555*, 643–646. https://doi.org/10.1038/nature26144

Clifford, S. M., & Parker, T. J. (2001). The evolution of the Martian hydrosphere: Implications for the fate of a primordial ocean and the current state of the northern plains. *Icarus*, *154*, 40–79.

Colombera, L., Mountney, N. P., & McCaffrey, W. D. (2015). A meta-study of relationships between fluvial channel-body stacking pattern and aggradation rate: Implications for sequence stratigraphy. *Geology*, *43*, 283–286. https://doi.org/10.1130/G36385.1

Craddock, R. A., & Howard, A. D. (2002). The case for rainfall on a warm, wet early Mars. *J Geophy Res*, *107*(E11), 21-1–21-36. https://doi.org/10.1029/2001JE001505

Davis, J. M., Balme, M. R., Grindrod, P. M., Williams, R. M. E., & Gupta, S. (2016). Extensive Noachian fluvial systems in Arabia Terra: Implications for early Martian climate. *Geology*, *G38247*, 1. https://doi.org/10.1130/G38247.1

Davis, J. M., Grindrod, P. M., Fawdon, P., Williams, R. M. E., Gupta, S., & Balme, M. (2018). Episodic and declining fluvial processes in Southwest Melas Chasma, Valles Marineris. *Mars. J. Geophys. Res. Planets in press.*, *123*(10), 2527–2549. https://doi.org/10.1029/2018JE005710

Davis, J. M., Gupta, S., Balme, M., Grindrod, P. M., Fawdon, P., Dickeson, Z. I., & Williams, R. M. E. (2019). A diverse array of fluvial depositional systems in Arabia Terra: Evidence for mid-Noachian to Early Hesperian Rivers on Mars. *Journal of Geophysical Research Planets*, *124*, 1913–1934. https://doi.org/10.1029/2019JE005976

Di Achille, G., & Hynek, B. M. (2010). Ancient ocean on Mars supported by global distribution of deltas and valleys. *Nat. Geosci.*, *3*, 459–463. https://doi.org/10.1038/ngeo891

Di Pietro, I., Ori, G. G., Pondrelli, M., & Salese, F. (2018). Geology of Aeolis Dorsa alluvial sedimentary basin. *Mars. J. Maps*, *14*, 212–218. https://doi.org/10.1080/17445647.2018.1454350

DiBiase, R. A., Limaye, A. B., Scheingross, J. S., Fischer, W. W., & Lamb, M. P. (2013). Deltaic deposits at Aeolis Dorsa: Sedimentary evidence for a standing body of water on the northern plains of Mars. *Journal of Geophysical Research Planets*, *118*, 1285–1302. https://doi.org/10.1002/jgre.20100

Durkin, P. R., Hubbard, S. M., Holbrook, J., & Boyd, R. (2018). Evolution of fluvial meander-belt deposits and implications for the completeness of the stratigraphic record. *GSA Bull.*, *130*, 721–739. https://doi.org/10.1130/B31699.1

Edgar, L. A., Gupta, S., Rubin, D. M., Lewis, K. W., Kocurek, G. A., Anderson, R. B., et al. (2018). Shaler: In situ analysis of a fluvial sedimentary deposit on Mars [WWW Document]. *Sedimentology*, *65*(1), 96–122. https://doi.org/10.1111/sed.12370

Edgett, K. S. (2005). The sedimentary rocks of Sinus Meridiani: Five key observations from data acquired by the Mars Global Surveyor and Mars Odyssey orbiters. *Int. J. Mars Sci. Explor.*, *1*, 5–58. https://doi.org/10.1555/mars.2005.0002

El Maarry, M. R., Markiewicz, W. J., Mellon, M. T., Goetz, W., Dohm, J. M., & Pack, A. (2010). Crater floor polygons: Desiccation patterns of ancient lakes on Mars? *J Geophys Res*, *115*(E10), E10006. https://doi.org/10.1029/2010JE003609

Fassett, C. I., & Head, J. W. (2007). Layered mantling deposits in northeast Arabia Terra, Mars: Noachian-Hesperian sedimentation, erosion, and terrain inversion. *Journal of Geophysical Research*, *112*, E08002. https://doi.org/10.1029/2006JE002875

Fassett, C. I., & Head, J. W. (2008a). Valley network-fed, open-basin lakes on Mars: distribution and implications for Noachian surface and subsurface hydrology. *Icarus*, *198*, 37–56.

Fassett, C. I., & Head, J. W. (2008b). The timing of Martian valley network activity: Constraints from buffered crater counting. *Icarus*, *195*, 61–89. https://doi.org/10.1016/j.icarus.2007.12.009

Fassett, C. I., & Head, J. W. (2011). Sequence and timing of conditions on early Mars. *Icarus*, *211*, 1204–1214. https://doi.org/10.1016/j.icarus.2010.11.014

Fastook, J. L., & Head, J. W. (2015). Glaciation in the Late Noachian Icy Highlands: Ice accumulation, distribution, flow rates, basal melting, and top-down melting rates and patterns. *Planet. Space Sci.*, *106*, 82–98. https://doi.org/10.1016/j.pss.2014.11.028

Fawdon, P., Gupta, S., Davis, J. M., Warner, N. H., Adler, J. B., Balme, M. R., et al. (2018). The Hypanis Valles delta: The last highstand of a sea on early Mars? Earth Planet. *Sci. Lett.*, *500*, 225–241. https://doi.org/10.1016/j.epsl.2018.07.040

Fogg, G. E. (1986). Groundwater flow and sand body interconnectedness in a thick. *Multiple-Aquifer System. Water Resour. Res.*, *22*, 679–694. https://doi.org/10.1029/WR022i005p00679

Friend, P. F., Slater, M. J., & Williams, R. C. (1979). Vertical and lateral building of river sandstone bodies, Ebro Basin. *Spain. J. Geol. Soc.*, *136*, 39–46. https://doi.org/10.1144/gsjgs.136.1.0039

Golombek, M. P., Warner, N. H., Ganti, V., Lamb, M. P., Parker, T. J., Fergason, R. L., & Sullivan, R. (2014). Small crater modification on Meridiani Planum and implications for erosion rates and climate change on Mars: Small Crater Modification on Mars. *Journal of Geophysical Research Planets*, *119*, 2522–2547. https://doi.org/10.1002/2014JE004658

Goudge, T. A., Fassett, C. I., Head, J. W., Mustard, J. F., & Aureli, K. L. (2016). Insights into surface runoff on early Mars from paleolake basin morphology and stratigraphy. *Geology*, *44*, 419–422. https://doi.org/10.1130/G37734.1

Goudge, T. A., Milliken, R. E., Head, J. W., Mustard, J. F., & Fassett, C. I. (2017). Sedimentological evidence for a deltaic origin of the western fan deposit in Jezero crater, Mars and implications for future exploration. *Earth Planet. Sci. Lett.*, *458*, 357–365. https://doi.org/10.1016/j.epsl.2016.10.056

Grotzinger, J. P., Arvidson, R. E., Bell, J. F., Calvin, W., Clark, B. C., Fike, D. A., et al. (2005). Stratigraphy and sedimentology of a dry to wet eolian depositional system, Burns formation, Meridiani Planum. *Mars. Earth Planet. Sci. Lett.*, *240*, 11–72. https://doi.org/10.1016/j.epsl.2005.09.039

Grotzinger, J. P., Gupta, S., Malin, M. C., Rubin, D. M., Schieber, J., Siebach, K., et al. (2015). Deposition, exhumation, and paleoclimate of an ancient lake deposit, Gale crater, Mars. *Science*, *350*, aac7575. https://doi.org/10.1126/science.aac7575

Hackney, C., & Carling, P. (2011). The occurrence of obtuse junction angles and changes in channel width below tributaries along the Mekong River, south-east Asia: TRIBUTARY JUNCTION ANGLE AND CHANNEL WIDTH CHANGES BELOW CONFLUENCES. *Earth Surf. Process. Landf.*, *36*, 1563–1576. https://doi.org/10.1002/esp.2165

Halevy, I., & Head, J. W. (2014). Episodic warming of early Mars by punctuated volcanism. *Nat. Geosci*, *7*, ngeo2293. https://doi.org/10.1038/ngeo2293

Hartmann, W. K. (2005). Martian cratering 8. *Isochron refinement and the history of Martian geologic activity. Icarus*, *174*, 294–320.

Hayden, A. T., Lamb, M. P., Fischer, W. W., Ewing, R. C., McElroy, B. J., & Williams, R. M. E. (2019). Formation of sinuous ridges by inversion of river-channel belts in Utah, USA, with implications for Mars. *Icarus*, *332*, 92–110. https://doi.org/10.1016/j.icarus.2019.04.019

Hoke, M. R. T., & Hynek, B. M. (2009). Roaming zones of precipitation on ancient Mars as recorded in valley networks. *Journal of Geophysical Research*, *114*(E8), 2008JE003247. https://doi.org/10.1029/2008JE003247

Hoke, M. R. T., Hynek, B. M., & Tucker, G. E. (2011). Formation timescales of large Martian valley networks. *Earth Planet. Sci. Lett.*, *312*, 1–12. https://doi.org/10.1016/j.epsl.2011.09.053

Howard, A. D., Moore, J. M., & Irwin, R. P. (2005). An intense terminal epoch of widespread fluvial activity on early Mars: 1. Valley network incision and associated deposits. *J. Geophys. Res*, *110*(E12), E12S14. https://doi.org/10.1029/2005JE002459
Hughes, C. M., Cardenas, B. T., Goudge, T. A., & Mohrig, D. (2019). Deltaic deposits indicative of a paleo-coastline at Aeolis Dorsa, Mars. *Icarus*, *317*, 442–453. https://doi.org/10.1016/j.icarus.2018.08.009
Hynek, B. M., Arvidson, R., & Phillips, R. J. (2002). Geologic setting and origin of Terra Meridiani hematite deposits on Mars. *J Geophys Res*, *107*(E10), 5088. https://doi.org/10.1029/2002JE001891
Hynek, B.M., Di Achille, G., 2017. Geological map of the Meridiani Region.
Hynek, B. M., & Phillips, R. J. (2001). Evidence for extensive denudation of the Martian highlands. *Geology*, *29*, 407–410. https://doi.org/10.1130/0091-7613(2001)029<0407:EFEDOT>2.0.CO;2
Hynek, B. M., & Phillips, R. J. (2008). The stratigraphy of Meridiani Planum, Mars, and implications for the layered deposits' origin. *Earth Planet. Sci. Lett.*, *274*, 214–220. https://doi.org/10.1016/j.epsl.2008.07.025
Hynek Beach, M., & Hoke, M. R. T. (2010). Updated global map of Martian valley networks and implications for climate and hydrologic processes. *Journal of Geophysical Research*, *115*(E9), E09008. https://doi.org/10.1029/2009JE003548
Irwin, R. P., Craddock, R. A., & Howard, A. D. (2005). *Interior* channels in Martian valley networks: Discharge and runoff production. *Geology*, *33*, 489–492.
Irwin, R. P., & Howard, A. D. (2002). Drainage basin evolution in Noachian Terra Cimmeria, Mars. *Journal of Geophysical Research Planets*, *107*, 10–1–10–23. https://doi.org/10.1029/2001JE001818
Irwin, R. P., Howard, A. D., Craddock, R. A., & Moore, J. M. (2005). An intense terminal epoch of widespread fluvial activity on early Mars: 2. Increased runoff and paleolake development. *Journal of Geophysical Research*, *110*(E12), E12S15. https://doi.org/10.1029/2005JE002460
Jakosky, B. M., Slipski, M., Benna, M., Mahaffy, P., Elrod, M., Yelle, R., et al. (2017). Mars' atmospheric history derived from upper-atmosphere measurements of 38Ar/36Ar. *Science*, *355*, 1408–1410. https://doi.org/10.1126/science.aai7721
Jaumann, R., Neukum, G., Behnke, T., Duxbury, T. C., Eichentopf, K., Flohrer, J., et al. (2007). The high-resolution stereo camera (HRSC) experiment on Mars Express: Instrument aspects and experiment conduct from interplanetary cruise through the nominal mission. *Planet. Space Sci.*, *55*, 928–952. https://doi.org/10.1016/j.pss.2006.12.003
Kirk, R. L., Howington-Kraus, E., Rosiek, M. R., Anderson, J. A., Archinal, B. A., Becker, K. J., et al. (2008). Ultrahigh resolution topographic mapping of Mars with MRO HiRISE stereo images: Meter-scale slopes of candidate Phoenix landing sites. *J Geophy Res*, *113*, E00A24. https://doi.org/10.1029/2007JE003000
Kite, E. S., Howard, A. D., Lucas, A. S., Armstrong, J. C., Aharonson, O., & Lamb, M. P. (2015). Stratigraphy of Aeolis Dorsa, Mars: Stratigraphic context of the great river deposits. *Icarus*, *253*, 223–242. https://doi.org/10.1016/j.icarus.2015.03.007
Kneissl, T., van Gasselt, S., & Neukum, G. (2011). Map-projection-independent crater size-frequency determination in GIS environments—New software tool for ArcGIS. *Planet. Space Sci.*, *59*, 1243–1254. https://doi.org/10.1016/j.pss.2010.03.015
Kraal, E. R., Asphaug, E., Moore, J. M., Howard, A., & Bredt, A. (2008). Catalogue of large alluvial fans in Martian impact craters. *Icarus*, *194*, 101–110. https://doi.org/10.1016/j.icarus.2007.09.028
Kronyak, R. E., Kah, L. C., Edgett, K. S., VanBommel, S. J., Thompson, L. M., Wiens, R. C., et al. (2019). Mineral-filled fractures as indicators of multigenerational fluid flow in the Pahrump Hills member of the Murray Formation, Gale Crater. *Mars. Earth Space Sci.*, *6*, 238–265. https://doi.org/10.1029/2018EA000482
Léveillé, R. J., Bridges, J., Wiens, R. C., Mangold, N., Cousin, A., Lanza, N., et al. (2014). Chemistry of fracture-filling raised ridges in Yellowknife Bay, Gale Crater: Window into past aqueous activity and habitability on Mars. *Journal of Geophysical Research Planets*, *119*, 2398–2415. https://doi.org/10.1002/2014JE004620
Levy, J. S., Head, J. W., & Marchant, D. R. (2009). Thermal contraction crack polygons on Mars: Classification, distribution, and climate implications from HiRISE observations. *J Geophy Res*, *114*(E1), E01007. https://doi.org/10.1029/2008JE003273
Maizels, J. K. (1987). Plio-Pleistocene raised channel systems of the western Sharqiya (Wahiba). *Oman. Geol. Soc. Lond. Spec. Publ.*, *35*, 31–50. https://doi.org/10.1144/GSL.SP.1987.035.01.04
Malin, M. C., Bell, J. F., Cantor, B. A., Caplinger, M. A., Calvin, W. M., Clancy, R. T., et al. (2007). Context camera investigation on board the Mars Reconnaissance Orbiter. *J Geophy Res*, *112*(E5), E05S04. https://doi.org/10.1029/2006JE002808
Malin, M. C., & Edgett, K. S. (2003). Evidence for persistent flow and aqueous sedimentation on early Mars. *Science*, *302*, 1931–1934. https://doi.org/10.1126/science.1090544
Martínez, J. L. C., Pérez, L. C., Marcuello, A., Cazo, P. A., Carpio, M. M., & Bellmunt, F. (2010). Exhumed channel sandstone networks within fluvial fan deposits from the Oligo-Miocene Caspe Formation, South-east Ebro Basin (North-east Spain). *Sedimentology*, *57*, 162–189. https://doi.org/10.1111/j.1365-3091.2009.01096.x
McEwen, A. S., Eliason, E. M., Bergstrom, J. W., Bridges, N. T., Hansen, C. J., Delamere, W. A., et al. (2007). Mars Reconnaissance Orbiter's High Resolution Imaging Science Experiment (HiRISE). *J Geophys Res*, *112*(E5), E05S02. https://doi.org/10.1029/2005JE002605
McRae, L. E. (1990). Paleomagnetic isochrons, unsteadiness, and non-uniformity of sedimentation in Miocene fluvial strata of the Siwalik group, Northern Pakistan. *J. Geol.*, *98*, 433–456. https://doi.org/10.1086/629418
Miall, A. D. (1988). Reservoir heterogeneities in fluvial sandstones: Lessons from outcrop studies. *AAPG Bull.*, *72*, 682–697. https://doi.org/10.1306/703C8F01-1707-11D7-8645000102C1865D
Michael, G. G. (2013). Planetary surface dating from crater size–frequency distribution measurements: Multiple resurfacing episodes and differential isochron fitting. *Icarus*, *226*, 885–890. https://doi.org/10.1016/j.icarus.2013.07.004
Michael, G. G., & Neukum, G. (2010). Planetary surface dating from crater size–frequency distribution measurements: Partial resurfacing events and statistical age uncertainty. *Earth Planet. Sci. Lett.*, *294*, 223–229. https://doi.org/10.1016/j.epsl.2009.12.041
Mohrig, D., Heller, P. L., Paola, C., & Lyons, W. J. (2000). Interpreting avulsion process from ancient alluvial sequences: Guadalope-Matarranya system (northern Spain) and Wasatch Formation (western Colorado). *GSA Bull*, *112*, 1787–1803. https://doi.org/10.1130/0016-7606(2000)112 <1787:IAPFAA>2.0.CO;2
Moore, J. M. (1990). Nature of the mantling deposit in the heavily cratered terrain of northeastern Arabia, Mars. *Journal of Geophysical Research Solid Earth*, *95*, 14,279–14,289. https://doi.org/10.1029/JB095iB09p14279
Moore, J. M., & Howard, A. D. (2005). Large alluvial fans on Mars. *Journal of Geophysical Research Planets*, *110*(E4), E04005. https://doi.org/10.1029/2004JE002352
Moore, J. M., Howard, A. D., Dietrich, W. E., & Schenk, P. M. (2003). Martian layered fluvial deposits: Implications for Noachian climate scenarios. *Geophys. Res. Lett.*, *30*(24). https://doi.org/10.1029/2003GL019002
Murchie, S., Arvidson, R., Bedini, P., Beisser, K., Bibring, J.-P., Bishop, J., et al. (2007). Compact Reconnaissance Imaging Spectrometer for Mars (CRISM) on Mars Reconnaissance Orbiter (MRO). *Journal of Geophysical Research*, *112*(E5), E05S03. https://doi.org/10.1029/2006JE002682

Neukum, G., & Jaumann, R. (2004). HRSC: The High Resolution Stereo Camera of Mars Express. In A. Wilson (Ed.), *Mars Express: The scientific payload*, (pp. 17–35). Noordwiijk: ESA Publications Division.
Newsom, H. E., Lanza, N. L., Ollila, A. M., Wiseman, S. M., Roush, T. L., Marzo, G. A., et al. (2010). Inverted channel deposits on the floor of Miyamoto crater, Mars. *Icarus, MRO/HiRISE Studies of Mars*, *205*, 64–72. https://doi.org/10.1016/j.icarus.2009.03.030
Palumbo, A. M., & Head, J. W. (2018). Impact cratering as a cause of climate change, surface alteration, and resurfacing during the early history of Mars. *Meteorit. Planet. Sci.*, *53*, 687–725. https://doi.org/10.1111/maps.13001
Palumbo, A. M., Head, J. W., & Wordsworth, R. D. (2018). Late Noachian Icy Highlands climate model: Exploring the possibility of transient melting and fluvial/lacustrine activity through peak annual and seasonal temperatures. *Icarus*, *300*, 261–286. https://doi.org/10.1016/j.icarus.2017.09.007
Perron, J. T., Mitrovica, J. X., Manga, M., Matsuyama, I., & Richards, M. A. (2007). Evidence for an ancient Martian ocean in the topography of deformed shorelines. *Nature*, *447*, 840–843.
Phillips, R. J., Zuber, M. T., Solomon, S. C., Golombek, M. P., Jakosky, B. M., Banerdt, W. B., et al. (2001). Ancient geodynamics and global-scale hydrology on Mars. *Science*, *291*, 2587–2591. https://doi.org/10.1126/science.1058701
Pizzuto, J. E. (1987). Sediment diffusion during overbank flows. *Sedimentology*, *34*, 301–317. https://doi.org/10.1111/j.1365-3091.1987.tb00779.x
Platz, T., Michael, G., Tanaka, K. L., Jr, J. A. S., & Fortezzo, C. M. (2013). Crater-based dating of geological units on Mars: Methods and application for the new global geological map. *Icarus*, *225*(1), 806–827. https://doi.org/10.1016/j.icarus.2013.04.021
Ramirez, R. M., & Craddock, R. A. (2018). The geological and climatological case for a warmer and wetter early Mars. *Nat. Geosci.*, *11*, 230–237. https://doi.org/10.1038/s41561-018-0093-9
Rice, M., BellI, J. III, Gupta, S., Warner, N., Goddard, K., & Anderson, R. (2013). A detailed geologic characterization of Eberswalde Crater, Mars. *Int. J. Mars Sci. Explor.*, *8*, 15–57.
Robbins, S. J., & Hynek, B. M. (2012). A new global database of Mars impact craters ≥1 km: 2. Global crater properties and regional variations of the simple-to-complex transition diameter. *Journal of Geophysical Research Planets*, *117*(E6). https://doi.org/10.1029/2011JE003967
Sadler, P. M. (1981). Sediment accumulation rates and the completeness of stratigraphic sections. *J. Geol.*, *89*, 569–584. https://doi.org/10.1086/628623
Schwenzer, S. P., Bridges, J. C., Wiens, R. C., Conrad, P. G., Kelley, S. P., Leveille, R., et al. (2016). Fluids during diagenesis and sulfate vein formation in sediments at Gale crater, Mars. *Meteorit. Planet. Sci.*, *51*, 2175–2202. https://doi.org/10.1111/maps.12668
Segura, T. L., Toon, O. B., Colaprete, A., & Zahnle, K. (2002). Environmental effects of large impacts on Mars. *Science*, *298*, 1977–1980.
Siebach, K. L., & Grotzinger, J. P. (2014). Volumetric estimates of ancient water on Mount Sharp based on boxwork deposits, Gale Crater, Mars. *Journal of Geophysical Research Planets*, *119*, 189–198. https://doi.org/10.1002/2013JE004508
Singh, A., Thomsen, K. J., Sinha, R., Buylaert, J.-P., Carter, A., Mark, D. F., et al. (2017). Counter-intuitive influence of Himalayan river morphodynamics on Indus Civilisation urban settlements. *Nat. Commun.*, *8*, 1–14. https://doi.org/10.1038/s41467-017-01643-9
Smith, D. E., Zuber, M. T., Frey, H. V., Garvin, J. B., Head, J. W., Muhleman, D. O., et al. (2001). Mars orbiter laser altimeter: Experiment summary after the first year of global mapping of Mars. *J Geophys Res*, *106*, 23,689–23,722.
Squyres, S. W., & Knoll, A. H. (2005). Sedimentary rocks at Meridiani Planum: Origin, diagenesis, and implications for life on Mars. *Earth Planet. Sci. Lett.*, *240*, 1–10. https://doi.org/10.1016/j.epsl.2005.09.038
Tanaka, K. L., Robbins, S. J., Fortezzo, C. M., Skinner, J. A. Jr., & Hare, T. M. (2014). The digital global geologic map of Mars: Chronostratigraphic ages, topographic and crater morphologic characteristics, and updated resurfacing history. *Planet. Space Sci.*, *95*, 11–24. https://doi.org/10.1016/j.pss.2013.03.006
Toon, O. B., Segura, T., & Zahnle, K. (2010). The formation of Martian river valleys by impacts. *Annu. Rev. Earth Planet. Sci.*, *38*, 303–322. https://doi.org/10.1146/annurev-earth-040809-152354
Vago, J. L., Westall, F., Pasteur Instrument Teams, L. S. S. W. G., Contributors, O., Coates, A. J., Jaumann, R., et al., & the ExoMars Project Team (2017). Habitability on Early Mars and the search for biosignatures with the ExoMars Rover. *Astrobiology*, *17*, 471–510. https://doi.org/10.1089/ast.2016.1533
Warner, N. H., Gupta, S., Calef, F., Grindrod, P., Boll, N., & Goddard, K. (2015). Minimum effective area for high resolution crater counting of Martian terrains. *Icarus*, *245*, 198–240.
Williams, R. M. E., Chuang, F. C., & Berman, D. C. (2017). Multiple surface wetting events in the greater Meridiani Planum region, Mars: Evidence from valley networks within ancient cratered highlands. *Geophys. Res. Lett.*, *44*, 1669–1678. https://doi.org/10.1002/2016GL072259
Williams, R. M. E., Grotzinger, J. P., Dietrich, W. E., Gupta, S., Sumner, D. Y., Wiens, R. C., et al. (2013). Martian fluvial conglomerates at Gale Crater. *Science*, *340*, 1068–1072. https://doi.org/10.1126/science.1237317
Williams, R. M. E., Irwin, R. P., Burr, D. M., Harrison, T., & McClelland, P. (2013). Variability in Martian sinuous ridge form: Case study of Aeolis Serpens in the Aeolis Dorsa, Mars, and insight from the Mirackina paleoriver, South Australia. *Icarus*, *225*, 308–324. https://doi.org/10.1016/j.icarus.2013.03.016
Williams, R. M. E., Irwin, R. P., Zimbelman, J. R., Chidsey, T. C., & Eby, D. E. (2011). Field guide to exhumed paleochannels near Green River, Utah: Terrestrial analogs for sinuous ridges on Mars. *Geol. Soc. Am. Spec. Pap.*, *483*, 483–505. https://doi.org/10.1130/2011.2483(29)
Williams, R. M. E., Moersch, J. E., & Fergason, R. L. (2018). Thermophysical Properties of Martian Fluvial Sinuous Ridges: Inferences on 'Inverted Channel' Induration Agent. *Earth Space Sci.*, *5*(9), 516–528. https://doi.org/10.1029/2018EA000402
Wordsworth, R., Forget, F., Millour, E., Head, J. W., Madeleine, J.-B., & Charnay, B. (2013). Global modeling of the early Martian climate under a denser CO2 atmosphere: Water cycle and ice evolution. *Icarus*, *222*, 1–19. https://doi.org/10.1016/j.icarus.2012.09.036
Wordsworth, R. D., Kerber, L., Pierrehumbert, R. T., Forget, F., & Head, J. W. (2015). Comparison of "warm and wet" and "cold and icy" scenarios for early Mars in a 3-D climate model: WARM AND WET VS. COLD AND ICY EARLY MARS. *Journal of Geophysical Research Planets*, *120*, 1201–1219. https://doi.org/10.1002/2015JE004787
Zabrusky, K., Andrews-Hanna, J. C., & Wiseman, S. M. (2012). Reconstructing the distribution and depositional history of the sedimentary deposits of Arabia Terra, Mars. *Icarus*, *220*, 311–330. https://doi.org/10.1016/j.icarus.2012.05.007
Zaki, A. S., Pain, C. F., Edgett, K. S., & Giegengack, R. (2018). Inverted stream channels in the Western Desert of Egypt: Synergistic remote, field observations and laboratory analysis on Earth with applications to Mars. *Icarus*, *309*, 105–124. https://doi.org/10.1016/j.icarus.2018.03.001